frontiers in Earth Science

ORIGINAL RESEARCH
published: 21 March 2022
doi: 10.3389/feart.2022.851737

# Earthquake Occurrences of the Major Tectonic Terranes for the Arabian Shield and Their Seismic Hazard Implications

*Sherif M. Ali*[1,2]* *and Kamal Abdelrahman*[3]

[1]National Research Institute of Astronomy and Geophysics (NRIAG), Cairo, Egypt, [2]Preparatory Commission for the Comprehensive Nuclear-Test-Ban Treaty Organization (CTBTO), International Data Centre (IDC), Vienna, Austria, [3]Department of Geology and Geophysics, College of Science, King Saud University, Riyadh, Saudi Arabia

The Arabian Shield, which contains a group of diverse terranes accreted during the Late Proterozoic, has experienced considerable historical and recent earthquake activities. From north to south, the Midyan terrane, Tabuk-Neom area, Hijaz terrane, Jeddah terrane, and Asir terrane make up the western section of the Arabian shield. In order to determine the earthquake occurrences and earthquake recurrence characteristics in the study area, an earthquake dataset containing 2,991 seismic events recorded between 1941 and 2019 with magnitudes of 1.0 and 6.2 and depths between 0 and 50 km was examined. The data were compiled by combining phase readings and information, such as origin times, hypocenter parameters, and magnitudes reported by the International Seismological Centre. The maximum likelihood method has been applied to calculate the Gutenberg–Richter recurrence parameters (a- and b-values) and magnitudes of completeness (Mc). The range of b-values is 0.53–1.04, which indicates that the study region experienced different stress level accumulations that cause earthquakes with different magnitudes. The Hijaz terrane is characterized by a high b-value (1.04 ± 0.34), which indicates a relatively low stress regime that resulted from the earthquakes stress release. The Midyan terrane is characterized by a low b-value (0.53 ± 0.10), which could be indicative of a relatively higher stress regime associated with a dominantly extensional stress. Mc values were found to be 1.4 in Midyan and Jeddah terranes. The lower value of Mc at Midyan terrane demonstrates appropriate station distribution and high earthquake rates. However, at Jeddah terrane, the seismic activities are poorly detected that probably lead to the small value of Mc. Higher Mc are evident in Hijaz terrane (Mc = 2.3) and Tabuk-Neom (Mc = 2.4), where the station distribution is very poor. The maximum expected magnitudes (Mmax) are found to be 6.0 for Midyan terrane, 5.4 for Tabuk-Neom, 4.7 for Hijaz terrane, 4.8 for Jeddah terrane, and 7.7 for Asir terrane. The average recurrence intervals of earthquakes with the Mmax are ~7, ~20, ~6, ~120, and ~200 years for each seismic terrain,

OPEN ACCESS

**Edited by:**
*Ahmed M. Eldosouky,*
*Suez University, Egypt*

**Reviewed by:**
*Melouah Oualid,*
*University of Ouargla, Algeria*
*Franck Eitel Kemgang Ghomsi,*
*National Institute of Cartography, Cameroon*
*Erdinc Oksum,*
*Süleyman Demirel University, Turkey*
*Mostafa Toni,*
*Helwan University, Egypt*

***Correspondence:**
*Sherif M. Ali*
*sherifmohamed.ali@hotmail.com*

**Specialty section:**
*This article was submitted to Solid Earth Geophysics, a section of the journal Frontiers in Earth Science*

**Received:** *10 January 2022*
**Accepted:** *08 February 2022*
**Published:** *21 March 2022*

**Citation:**
*Ali SM and Abdelrahman K (2022) Earthquake Occurrences of the Major Tectonic Terranes for the Arabian Shield and Their Seismic Hazard Implications. Front. Earth Sci. 10:851737. doi: 10.3389/feart.2022.851737*

**Abbreviations:** NRIAG, National Research Institute of Astronomy and Geophysics; CTBTO, Preparatory Commission for the Comprehensive Nuclear-Test-Ban Treaty Organization; IDC, International Data Centre; ISC, The International Seismological Centre; Mc, magnitudes of completeness; Mmax, the maximum expected magnitudes; G–R, the Gutenberg–Richter relationship; FMD, frequency–magnitude distributions.

respectively. The probability of occurrence and returned periods of different magnitudes in each region indicate that regions related to the Najd strike-slip fault system are the regions for large probable earthquake occurrences.

**Keywords: seismicity, magnitude of completeness (Mc), b-value, the International Seismological Centre (ISC), seismic hazard, Arabian Shield**

## 1 INTRODUCTION

The Arabian Plate, bounded by relatively active tectonic regions is characterized by dominant earthquake activities (Girdler, 1991; Al-Haddad et al., 1994; Ghebreab, 1998; Stern and Johnson, 2010; Al-Amri, 2013; Youssef, 2015). The Dead Sea transform fault bounds the Arabian Plate on the northwest and extends from southern Turkey in the north through Syria and the Dead Sea to the Gulf of Aqaba. A rise to the Turkish–Iranian Plateau due to the collision between the Eurasian Plate and the Arabian Plate has led to convergent boundaries, which border the Arabian Plate from the east and the north, while at the west (the Red Sea) and the south (Gulf of Aden), divergent margins originated as a result of sea floor spreading and rifting (**Figure 1**).

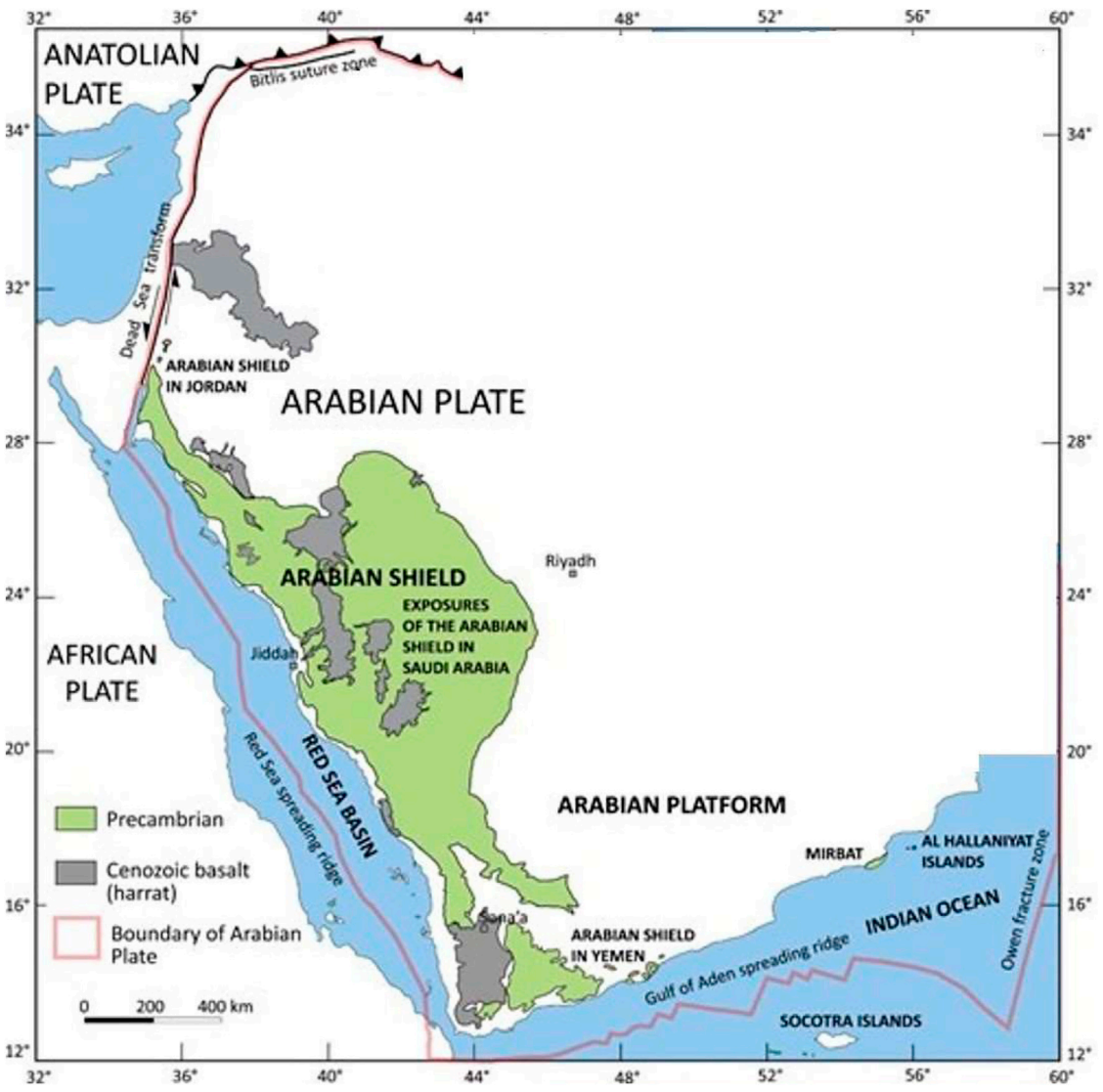


**FIGURE 1 |** The Arabian Plate, showing outcrops of Neoproterozoic and older rocks in the Arabian Shield and Oman, Cenozoic basalt associated with the opening of the Red Sea, and the plate boundaries—extensional in the south and west, convergent in the north and northeast, and transcurrent in the northwest and southeast (https://sgs.org.sa/en/ topics/landforms-of-saudi-arabia/).

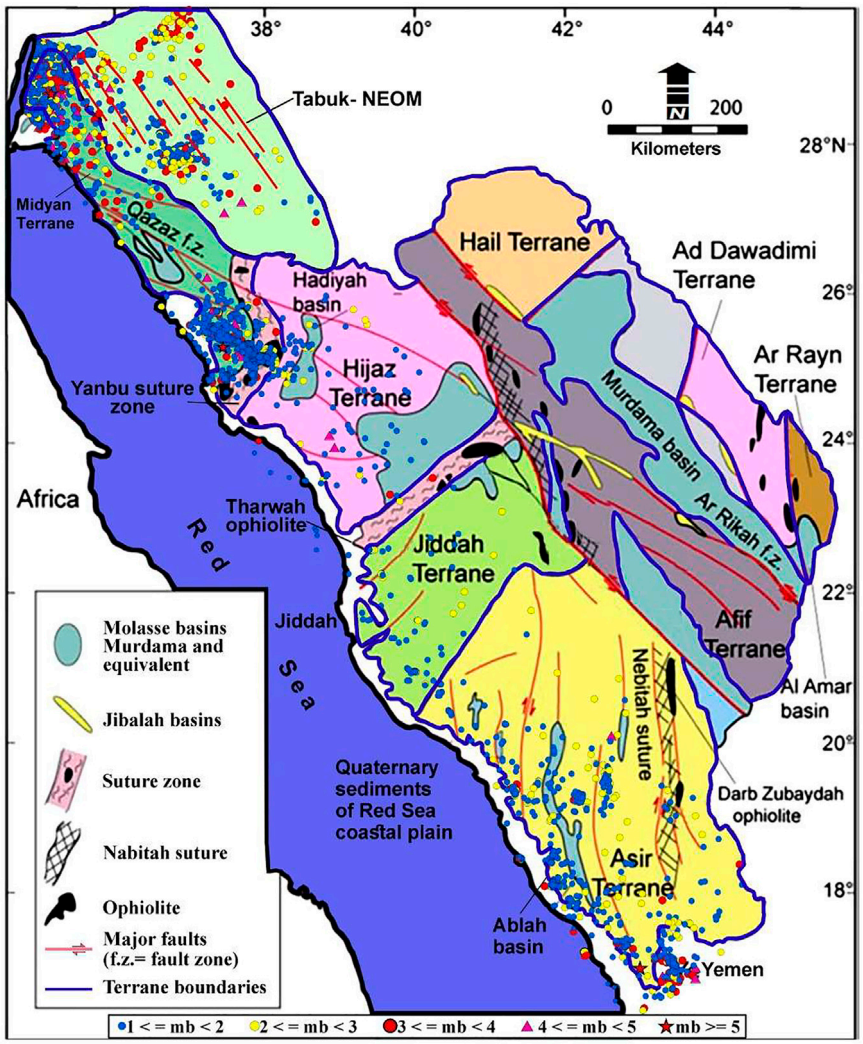


**FIGURE 2 |** Geologic map of the Arabian Shield showing the major geologic terranes and their boundaries, Najd fault system, and sedimentary basins (modified after Al-Amri et al., 2004) and the seismic activity from 1980 to 2019 using the International Seismological Centre catalog (ISC, 2021).

In the past, the Arabian shield experienced considerable earthquake records (Ambraseys and Adams, 1988; Ambraseys and Melville, 1988, 1989). However, it has incomplete pre-instrumental earthquakes activities due to sparse population, which reveal the prominent tectonic activities in the Cenozoic. During the last century, several moderate-sized to large earthquakes shock the area and the adjacent territories. Two large magnitude earthquakes were recorded on January 11, 1941 and November 22, 1995 with magnitudes of MS = 6.5 and MW = 7.3, respectively (Ambraseys et al., 1994; Klinger et al., 1999). The seismic sources are divided into three types including active geological faults, area source zones, and smoothed seismicity. The active fault is the dominant, especially when the magnitude and focal mechanism are well recognized.

The Arabian Shield, a prehistoric land mass with a trapezoidal shape is surrounded by Phanerozoic sediments and separated from the Red Sea by tight coastal plain of Cenozoic sediments (Kroner, 1985). It is a stable craton, which comprises a crystalline basement, predominantly metavolcanic, metasedimentary, and plutonic rocks of Precambrian continental crust of about 40–45 km thick (Davidson et al., 1994; Genna et al., 2002). Its slightly arched surface is a peneplain sloping very gently toward the north, northeast, and east.

The accumulation of oceanic island arcs along suture zones defined by ophiolites forms the Arabian shield (Stoeser and Camp, 1985). The accretion produces tectonostratigraphic terranes, which are divided by significant suture zones oriented north and northeast, and lined by serpentinite ultramafic rocks (tectonic slices and ophiolites) or major NW trending faults (**Figure 2**). The Midyan terrane, the Tabuk-Neom area, the Hijaz terrane, the Jeddah terrane, and the Asir terrane formed the western half of the Arabian Shield, from north to south (Johnson, 1998; Stern and Johnson, 2010). These terranes are separated by major suture zones, namely, Yanbu, Bi'r Umq, Afif, Nabitah, and Al Amar suture zones.

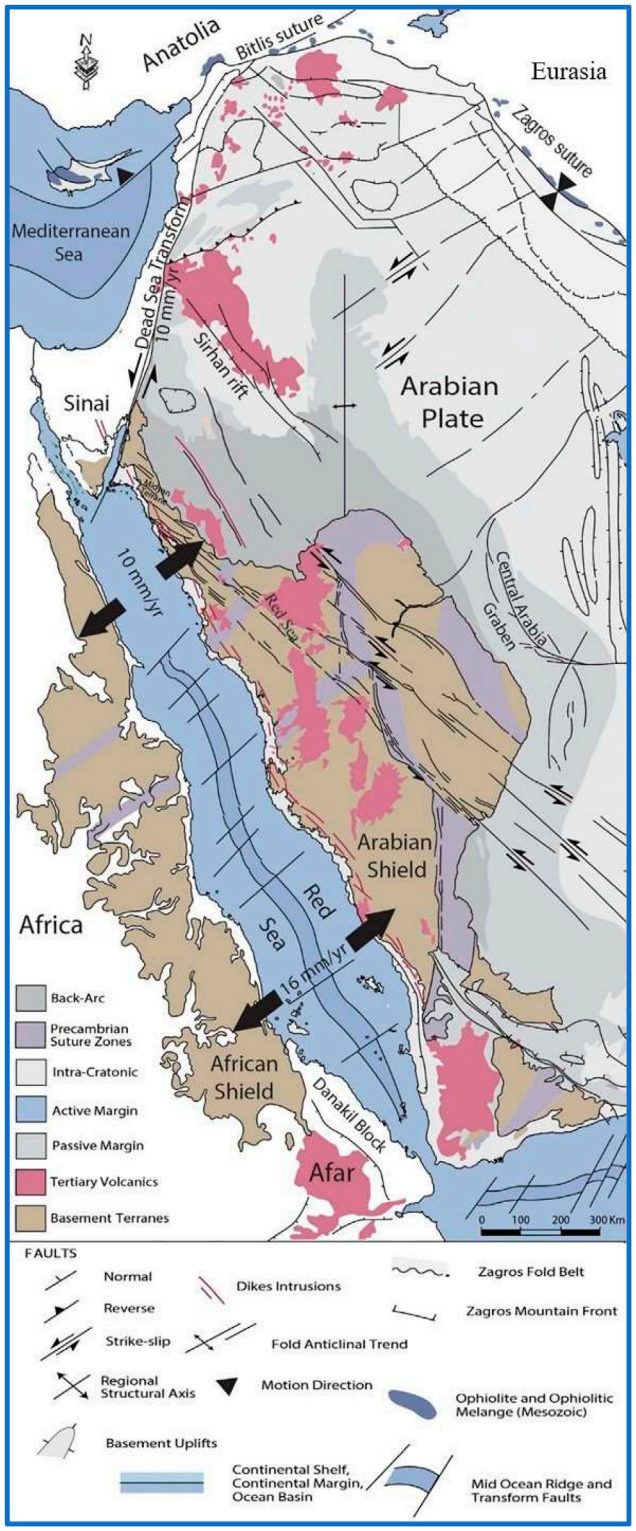


**FIGURE 3 |** Geological and tectonic elements map of the Arabian Plate and surrounding regions modified after Sharland et al. (2001). Geodetic observations estimate extensional rates along the Red Sea between 7 and 15 mm/year from north to south, and between 15 and 19 mm/year from west to east, left lateral slip rates along the southern Dead Sea Transform in (*Continued*)

**FIGURE 3 |** the range of 4.5–4.7 mm/year (e.g., ArRajehi et al., 2010). Counterclockwise rotation of Arabia relative to Eurasia was reported after Reilinger et al. (2006) in the range of 20–30 mm/year, leading to left lateral strike slip (East Anatolian Fault) along the northern boundary of the Arabian Plate with GPS slip rates in the range of 17–24 mm/year from east to west Turkey. The slip rates increase eastward along the Zagros mountain belts from 18 to 25 mm/year (Walpersdorf et al., 2006).

Aldaajani et al., 2021 stated that, at the northern boundary of the Arabian Plate, the boundary forces seem to have changed from compression to strike-slip style, due to the oblique collision between Anatolian and Arabian plates, which led to lateral escape tectonics of the Anatolian Plate (**Figure 3**) (Reilinger et al., 2006). This may have occurred simultaneously with the crustal extension in the Red Sea. Following the collision of Arabia and Eurasia and the Red Sea initiation, the strength contrast between Afro-Arabia continent and the oceanic lithosphere of the Mediterranean may have initiated movement along the Dead Sea Transform soon after a dike intrusion event along the western margin of the Arabian Plate (ArRajehi et al., 2010). This ultimately resulted in the development of the Sinai microplate (Beydoun, 1999).

The purpose of this study is to characterize the seismic activities related to these main terrains in the Arabian Shield. Furthermore, the study aims to indicate the dominant tectonic regimes of the studied regions and identify their related faulting types as well as characterize the earthquake rate changes and the risk of higher magnitude earthquakes related to each terrane, and obtain some seismicity parameters [a- and b-values and magnitude of completeness (Mc)]and seismic hazard parameters (earthquake recurrence and maximum expected magnitude) to be able to perform actions for seismic risk reduction in the studied region.

## 2 TECTONIC ENVIRONMENTS

Saudi Arabia occupies the majority of the Arabian plate that was formed between 25 and 30 million years ago. Because of rifting along the northeastern African continent's boundary, the Red Sea, and the Gulf of Aden opening, the rocks that make up the Arabian Peninsula, Jordan, Syria, Iraq, and westernmost Iran are found to split up from the African continent. Although the plate is a relatively new tectonic unit, it combines materials that have formed over a long period of geologic time. These rocks comprise a 45-km-thick layer of continental crust. Because of Mesozoic and Cenozoic uplift, Precambrian rocks are exposed toward southwest of the plate. In other places, the Precambrian rocks are obscured by a low-dipping succession of Phanerozoic deposits, which can be more than 10-km thick in the Arabian Gulf (Johnson, 1998). Precambrian shields typically have sufficiently thick and cold lithosphere that mantle earthquakes could occur. Their exceedingly low strain rates, including those within Arabia, cause mantle earthquakes to be particularly rare beneath shields (Frohlich et al., 2015). Volcano-seismicity, with mantle and lower-crustal earthquakes likely caused by early-stage

pooling and mixing of asthenospheric melt at the base of or within the lower-crust, are also rare in cratons, including Arabia, given their low heat flow (Prieto et al., 2017).

Tectonically, the movement of the Arabian plate northeast away from Egypt and Sudan is accompanied by compression and strike-slip displacement along the Zagros and Bitlis zones, and by strike-slip faulting along the Dead Sea transform. The northern part of the Arabian plate moves northwest toward the Eurasian plate with a rate of 20 ± 3 mm/year (Johnson, 1998; Jamali et al., 2006). The tectonic pattern of the western Arabia is congenital from the basement tectonics of ancient Nubian–Arabian shield, which received its main structural imprint during late Precambrian orogenic stages. The most important tectonic features are the NW-SE strike faults parallel to the extension of the Red Sea, Gulf of Suez rift, Aqaba fault trend, Najd faults system, NE-SW, and E-W (Tethyan trend) that affect the north and the NW Red Sea region.

The Najd strike-slip fault system is the Arabian shield's most notable structural feature. It extends in a zone >1,200 km in length and >300 km wide over the north-eastern Arabian Shield. This faults trend NW-SE with strike lengths >500 km, small sinistral displacements <25 km, and cumulative displacement across the zone >240 km. The Najd system's shear zones separate the western and eastern geologic terranes. From the NE coast of the Red Sea to the SE shield area, where the fault system is hidden beneath Mesozoic sedimentary strata, at least four major NW-SE trending left-lateral wrench zones of Najd intersect the shield. On the Najd system, cumulative Precambrian left-slip fault is estimated to be around 240 km (Brown, 1970). The Arabian Shield is made up of metamorphosed rocks that are overlain by a thick succession of Phanerozoic sedimentary rocks to the east, north, and south, and the Red Sea to the west. The shield's rocks are mostly Cenozoic basaltic volcanic lava fields, known as Harrat (an active volcanic field located along the western edge of the Arabian Shield, east of the Red Sea rift margin, beneath which earthquakes occurred within the lithospheric mantle), whereas those to the west of it are Cenozoic rocks from the Red Sea basin. The Red Sea and Gulf of Aden basins and phanerozoic rocks are typically slightly deformed and impacted by block faulting and open folds. The western and southern edges of the Arabian Plate were uplifted and partly surrounded by subaerial flood basalt during the previous 25 million years, culminating in the development of the Red Sea Cliff and Harrat (Davidson et al., 1994).

## 3 SEISMICITY OF THE ARABIAN SHIELD

The Arabian Plate has a clustered seismicity along the Dead Sea transform fault, the Red Sea rifting, Zagros fold and thrust belt, Makran subduction zone and Biltis thrust. Along the Red Sea rifting, the Gulf of Aden and Gulf of Aqaba, seismic activity is largely controlled and confined. It is concentrated near the axial trough of the Red Sea (Al-Malki and Al-Amri, 2013).

The spreading of the Red Sea floor and volcanism are linked to the distribution of earthquakes in the western half of the Arabian Shield. Several moderate-sized earthquakes struck the Arabian

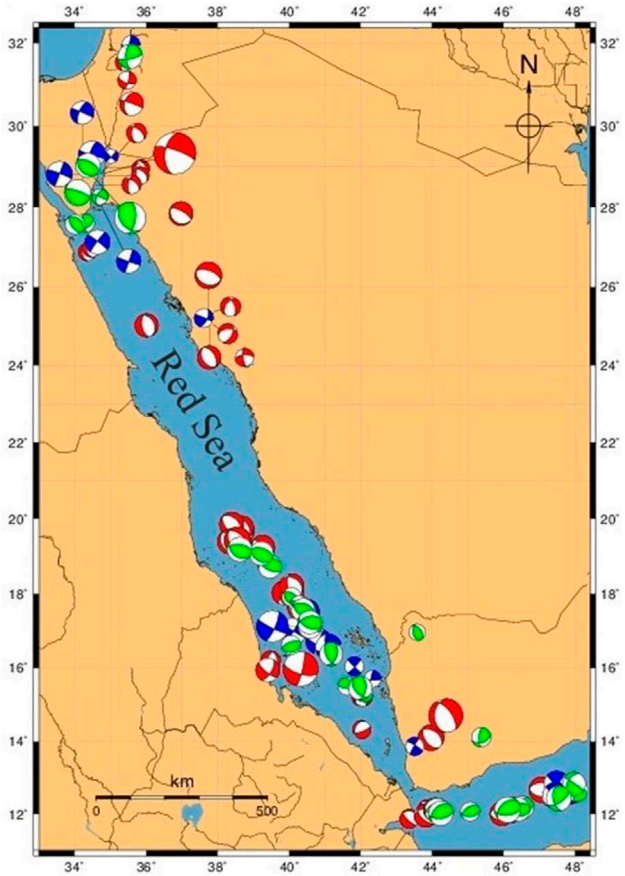


**FIGURE 4 |** Focal mechanism solutions of the 122 earthquakes in the Arabian Shield and its surrounding regions during the period from 1977 to 2021. Normal faulting solutions (in red). Strike-slip solutions (in blue) and thrusting solutions (in green). Size of focal sphere is proportional to magnitude.

Peninsula's extreme southwest. On January 11, 1941, near the modern Saudi Arabia–Yemen border, one of the greatest occurrences of magnitude Ms = 6.5 happened. It resulted in the deaths of several hundreds of people and the destruction of 1,700 buildings, 300 of which were destroyed, and 400 were severely damaged (Ambraseys et al., 1994). On January 23, 2014, an earthquake sequence was recorded around 50 km northeast of Jizan city, with the greatest occurrence having a local magnitude of Ml = 5.1 (El-Hadidy et al., 2015; Youssef, 2015). The earthquake fault plane solution indicates mainly a strike-slip northeast–southwest faulting mechanism, which, together with the aftershock distribution, matches the known NE-SW faults.

The northwestern Arabian Shield is characterized by strong historical earthquakes (Ambraseys and Melville, 1989; El-Isa and Al Shanti, 1989); the largest earthquake took place in AD 1068 with an intensity ~IX. It caused nearly 20,000 deaths and huge damages in Tabuk City, the Sinai Peninsula, and near the Dead Sea (Ambraseys and Melville, 1989; El-Isa and Al Shanti, 1989). Many recent moderate-to-large earthquakes are located in the study area, including a series of earthquakes in June 2004, about

**TABLE 1 |** Number of earthquakes, magnitude, and depth ranges; seismicity and seismic hazard parameters for the studied regions in the Arabian Shield.

| Regions | Total no. of events | No. of events M ≥ 1.0 | Depth range (km) | Max mag | a-value | b-value | Mc | Mmax |
|---|---|---|---|---|---|---|---|---|
| Midyan terrane | 16,483 | 1,521 | 0–51 | 5.5 | 3.73 | 0.53 ± 0.10 | 1.4 ± 0.35 | 6.0 |
| Tabuk-NEOM | 1,012 | 899 | 0–35 | 4.9 | 4.35 | 0.76 ± 0.13 | 2.4 ± 0.48 | 5.4 |
| Hijaz terrane | 103 | 55 | 0–59 | 4.2 | 3.88 | 1.04 ± 0.34 | 2.3 ± 0.56 | 4.7 |
| Jeddah terrane | 114 | 68 | 0–19 | 4.3 | 2.70 | 0.70 ± 0.19 | 1.4 ± 0.38 | 4.8 |
| Asir terrane | 716 | 448 | 0–57 | 6.2 | 3.72 | 0.83 ± 0.23 | 1.6 ± 0.44 | 6.7 |

60 km southwest of Tabuk. The largest earthquake in this series took place on June 22, 2004 with a magnitude of Ml = 5.2. On August 27, 2009, an earthquake with a magnitude of Ml = 5.1 took place about 45 km north of Badr City. On May 19, 2009, the area was hit by an earthquake swarm in Harrat Lunayir with magnitudes of Ml = 5.4 for the main event, which was felt in Al Madinah (Youssef, 2015; Zahran et al., 2016).

## 4 FOCAL MECHANISM SOLUTIONS

Several approaches are used to understand the earthquake phenomena. One such approach is the focal mechanism solutions (FMS). The main purposes of focal mechanism analysis are to identify seismic faults from seismological observations and to study the type of displacement and the relative motion between the different plates' boundaries. The focal mechanism solutions, together with the distribution of seismic activity are very useful indicators for the seismotectonic setting, the earthquake generating processes, and the stress regime of a certain region. Determination of the focal mechanism solutions provides extensive information about the sense of fault movements and the state of stress in the lithosphere. In this study the most recently compiled focal mechanism dataset given for the Arabian Shield and surrounding regions are considered. Focal mechanism data were mainly obtained from the International Seismological Centre (ISC) catalog for the region from 12° to 32°N latitudes and between 34° and 48°E longitudes). The final compiled focal mechanisms catalog is comprised of a total number of 122 solutions spanning the time period from 1977 to 2021. These solutions, which are presented in **Figure 4**, demonstrate a majority of normal faulting mechanism. Some scarcely strike-slip and thrust faulting mechanism solutions are also noticed. The normal mechanism with centroid depths at 12–19 km, a strike-slip mechanism with centroid depths at 10–22 km and a thrust mechanism with centroid depths at 10–25. The focal mechanism solutions show a dominant extensional regime with almost horizontal NE-SW trending.

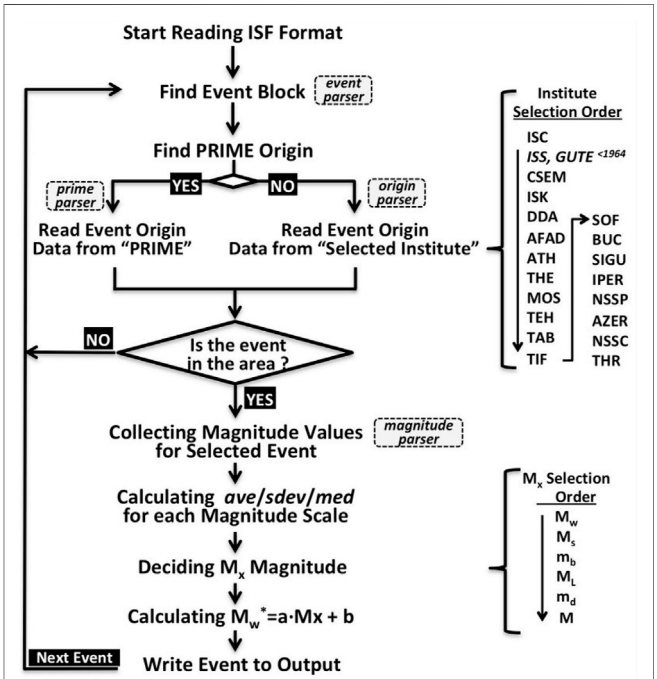


**FIGURE 5 |** Flowchart of the International Seismological Centre (ISC) database processing. Ave, average (mean); Med, median; Sdev, standard deviation. Mw is equivalent moment magnitude. See **Appendix A** for the institute codes.

## 5 ANALYSIS OF SEISMICITY PARAMETERS

### 5.1 Gutenberg–Richter relationship

The Gutenberg–Richter (G–R) relationship is the common recurrence relationship, which describes the seismicity of a seismic region. Once the earthquakes take place, the relationship between their frequency of occurrences and magnitude distributions (FMD) can be given by the following equation:

$$\log N(M) = a - b\,M \tag{1}$$

where the cumulative number of earthquakes N(M) is computed for all magnitudes M and greater. The a and b parameters are the seismicity constants that are indications for the seismic activity level and the slope of the FMD, respectively.

The a-value is the seismic activity rate that illustrates the above equation when it cuts across at M = 0. This variable parameter changes with the changes of seismic activity, the time, and term of observation, the earthquake magnitude, and the stress regime of the region under study (Gutenberg and Richter, 1944). With the increasing earthquake magnitudes in a region, the slope of its frequencies is determined by the b-value. It can also present the

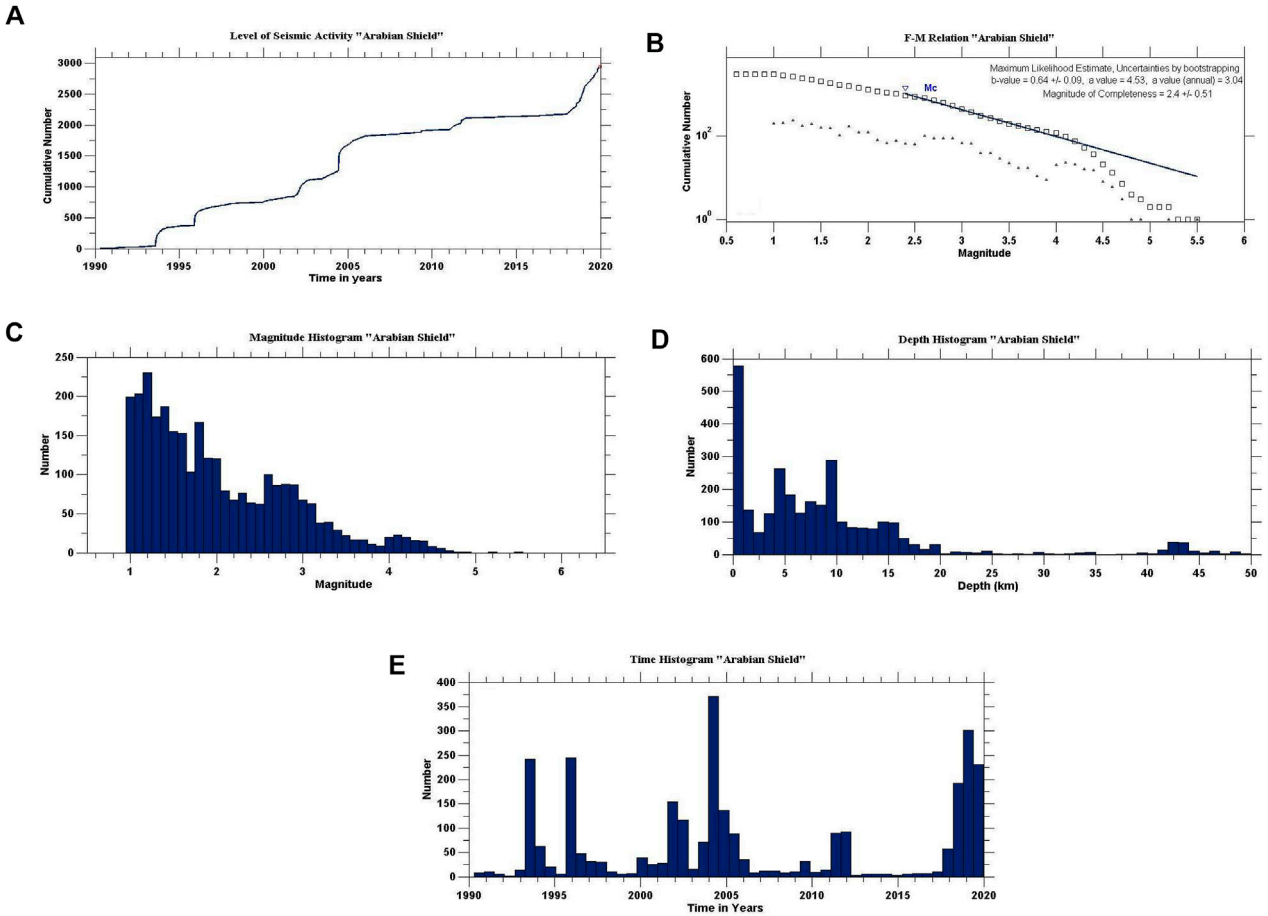


**FIGURE 6 |** The statistical analysis results of the Arabian Shield region using the whole dataset. **(A)** The evolutions among the levels of seismic activities, **(B)** the magnitude–frequency relationship, Mc is the cutoff magnitude (triangles and squares show earthquake numbers and the cumulative earthquakes for each magnitude value, respectively), **(C)** the magnitude histogram, **(D)** the depth distributions, and **(E)** the time histogram.

proportion of the earthquake sizes in numbers. The b-value is changing by the stress and strain distribution as well as the type of the rock. It is close to unity for most tectonically active regions (Schorlemmer et al., 2005). Areas with low heterogeneities (reduced geological complexity or crack density) and low thermal gradients are characterized by low b-values, while high heterogeneous regions, which are characterized by low velocity of deformation and less stress and strain, are the areas of higher b-values (Mogi, 1962; Manakou and Tsapanos, 2000). The correlation between b-values and the faulting mechanisms has been inferred from some previous studies, which relates normal faults to b-values ~1.1, strike-slip faults to b-values ~0.9, and thrust faults to b-value ~0.7 (Schorlemmer et al., 2005).

## 5.2 Magnitude of completeness

The magnitude of completeness (Mc) is defined as the lowest magnitude above which most of earthquakes are detected in space–time volume (Wiemer and Wyss, 2000; Ali and Shanker, 2017; Hafiez and Toni, 2020; Ali and Akkoyunlu, 2022). The accurate estimation of Mc is crucial, where increasing the values of Mc lead to take insufficient data and decreasing the Mc values lead to take a huge number of bogus data (Mignan and Woessner, 2012). The completeness magnitude is a basic requirement for modeling the seismicity in a region. The maximum curvature technique, the most reliable method to estimate Mc, is utilized to locate the maximum curvature point that refers to the magnitude of completeness by computing the first derivative maximum value of the slope of earthquake curve (Wiemer and Wyss, 2000).

There are various other methods to determine the magnitude of completeness. Some of these methods are the Mc by b−value stability, median-based analysis of the segment slope, and goodness-of-fit test. Although, the maximum curvature technique is easily applicable, Mc can be misjudged for the gradually curved FMDs. Consequently, utilizing other methods provide more reasonable estimates for Mc (Michael, 2014). When using more homogeneous local dataset, the maximum curvature technique gives more reasonable values for Mc (Mignan et al., 2011; Hafiez and Toni, 2020). The maximum curvature method requires less events compared with other methods, where uncertainties are also applicable by applying the Monte Carlo approach of the bootstrap technique (Efron, 1979). When the

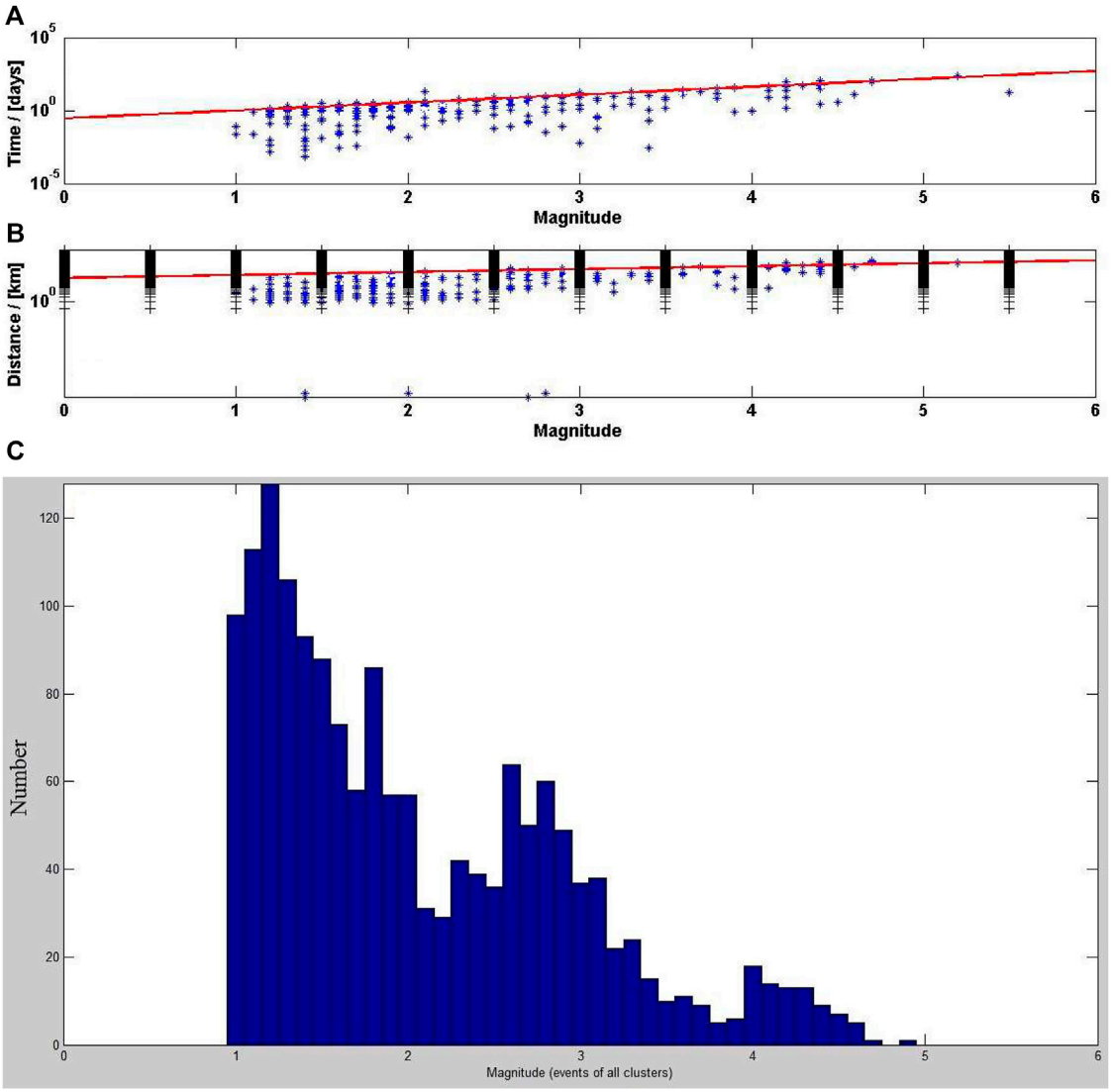


**FIGURE 7 |** Distribution of events through **(A)** time and **(B)** latitude for foreshock, mainshock, and aftershock sequences. **(C)** The magnitude histogram of the declustered catalog.

number of events is small, it leads to higher uncertainty values, and when the sample size is large enough (≥150 events), it allows a better estimation for Mc.

## 5.3 Seismic hazard parameters

The assessment of the previous earthquake distribution and their magnitudes in a seismotectonic region, as well as the calculation of the seismicity parameters, is the main stride to estimate the earthquake probability. The a- and b-values in the Gutenberg–Richter FMD can be employed to foresee the probability of future earthquakes of various magnitudes and recurrence intervals (Mogi, 1962; Scholz, 1968).

The earthquake probability of magnitude $M$ (in any period $T$) is calculated by the Poisson model, a base model to calculate the probabilistic seismic hazard that have been used in the maps of the National Earthquake Hazard (Frankel, 1995), in the California Seismic Hazard Maps (Petersen et al., 1996), and in fault lengths and global earthquakes (Leonard et al., 2001). This method is defined by the following equation:

$$P\ (M) = 1 - e^{-N(M)*T} \tag{2}$$

where $P\ (M)$ is the probability that at least one earthquake will take place within certain periods ($T$), $M$ is computed by **Eq. 1**. According to the Poisson model, the recurrence interval ($Q$) is given by the following equation:

$$Q = 1/N\,(M) \tag{3}$$

The relationship between the magnitude and reputed length (L) is employed for computations of the maximum expected earthquake magnitudes. The most likely magnitude for a certain maximum rupture is estimated by (L), which is not the maximum

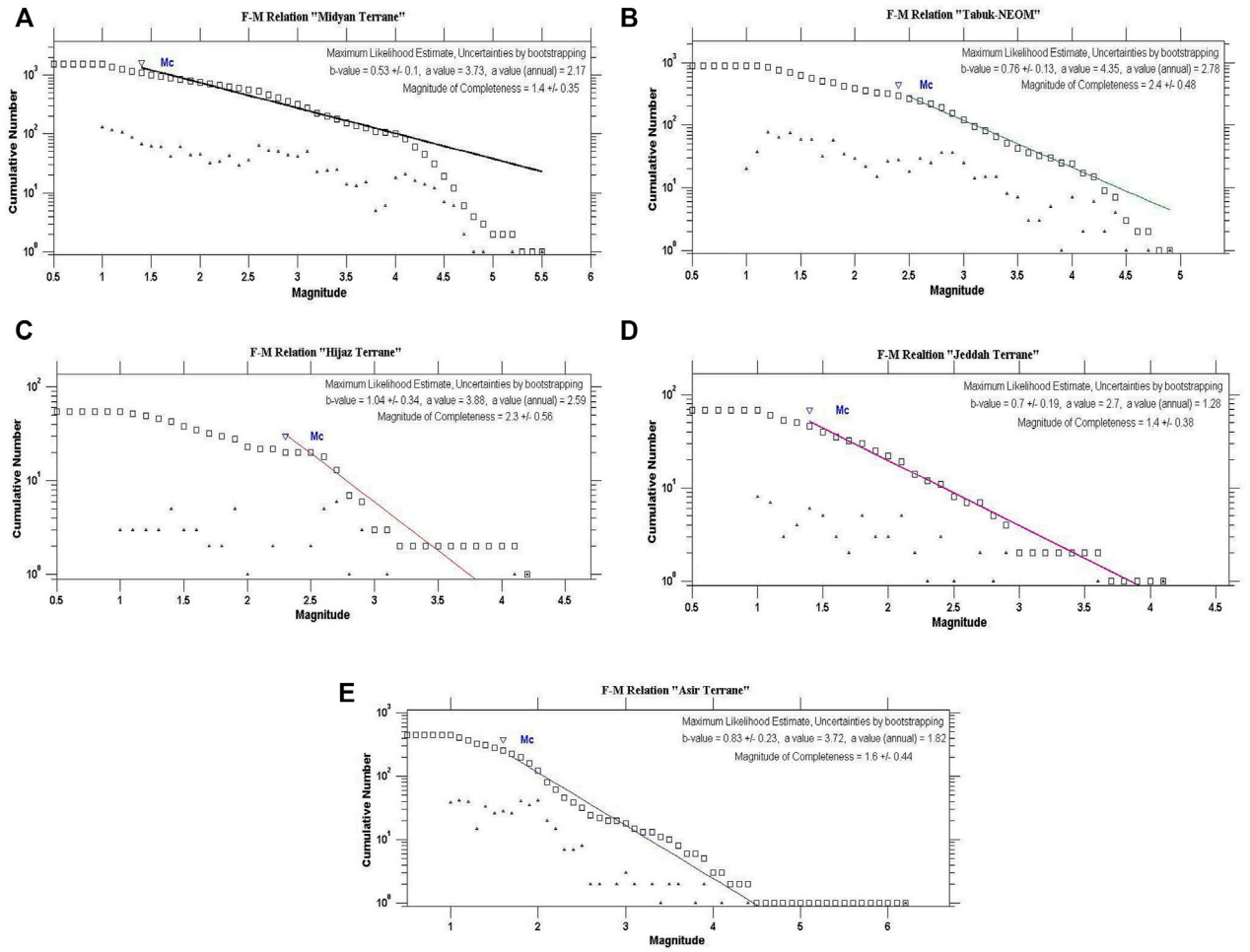


**FIGURE 8 | (A–E)** Frequency–magnitude relations of the studied seismic regions calculated by the maximum curvature technique. Mc is the cut-off magnitude (squares and triangles show the cumulative earthquakes for each magnitude value, as well as the earthquake numbers, respectively).

magnitude, but rather the magnitude that could be anticipated to overtake in half of the earthquakes correlated with that rupture length.

$$M = 5.08 + 1.16*\log(L) \quad (4)$$

It is possible to use the regression models to estimate the expected magnitude. Wells and Coppersmith (1994) used the documented and published historical and recent reports to take out relations between the rupture length and average surface displacement. The maximum expected magnitude (Mmax) was obtained by adding 0.5 units to the maximum observed magnitude (Kijko, 2004) (**Table 1**).

## 6 SEISMICITY CATALOG

The earthquake catalog is one of the most important outputs of seismology. It presents a broad dataset in earthquake events, which comprises the seismicity analysis in space–time volume, seismotectonic, and seismic hazard assessment (SHA). When the catalog has longer time span, the hazard parameters are well estimated (Rydelek and Sacks 1989; Wiemer and Wyss 2000; Woessner and Wiemer, 2005; Ali, 2016).

The initial earthquake catalog in the current study is compiled for the Arabian shield. It initially comprises 3,750 local earthquakes recorded during the period from 1941 to 2019 with magnitudes range from 1 to 6.2 and focal depths range from 0 to 50 km. This catalog is utilized to characterize seismicity of the study area. It is compiled by combining phase readings and information retrieved from regional seismological agencies and reported by the International Seismological Centre (ISC) online bulletin available at (http://earthquake.isc.ac.uk/). In examining the earthquake catalog completeness, the earthquake dataset used in the seismicity studies should use similar magnitude scales. The most recorded events in the study area have been reported by ISC in “ml” magnitude scale. Only few events are reported by other different magnitude scales, such as Md, mb, and/or Ms, which have been removed from our study for consistency. Therefore, a homogenous earthquake data catalog has been prepared using only one magnitude type “ml” (**Table 1**).

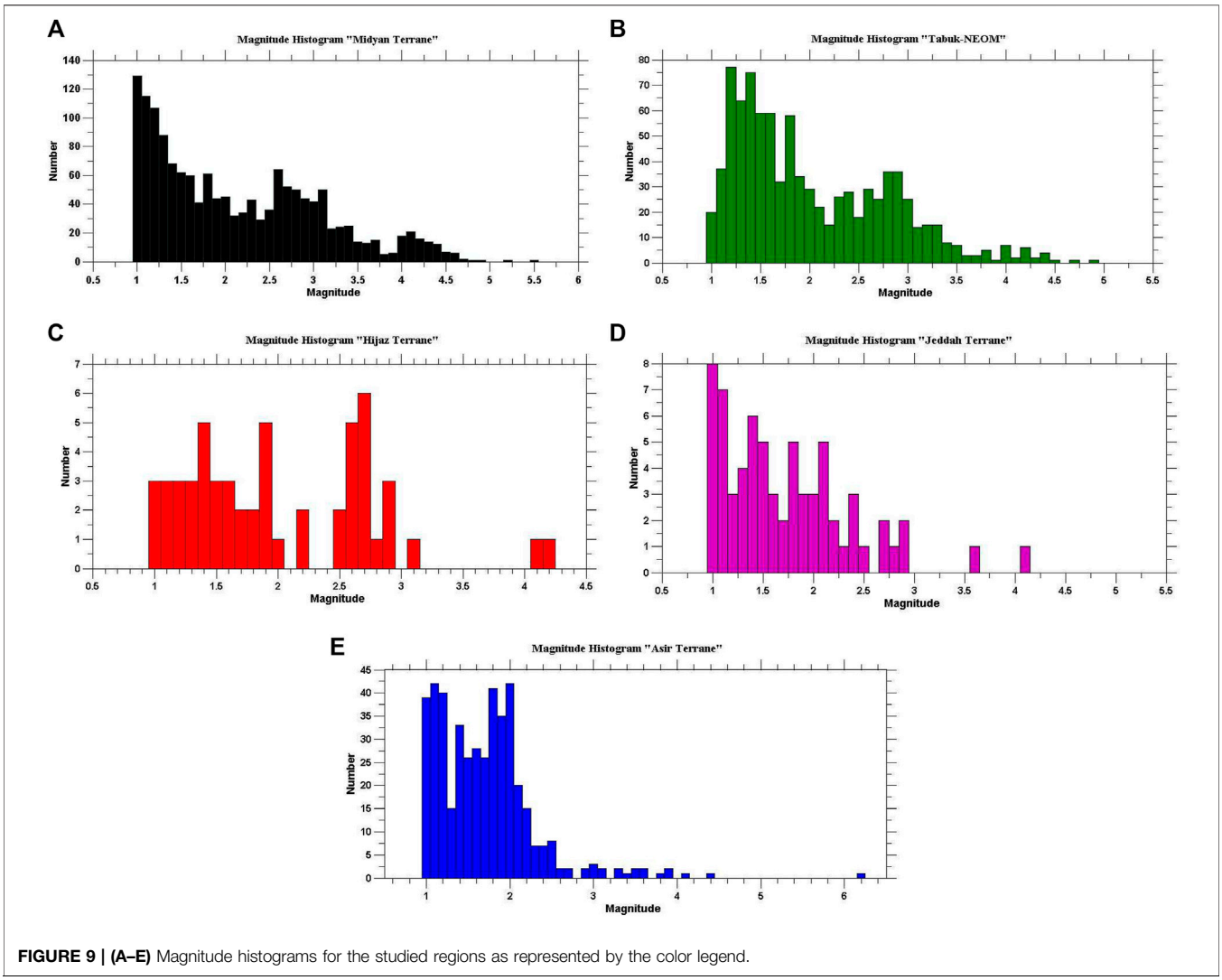


**FIGURE 9 | (A–E)** Magnitude histograms for the studied regions as represented by the color legend.

The ISC bulletin is one of the main sources of data for regional and global imaging of the Earth's tectonics and structure, and seismic hazard research work. The most important feature of the ISC bulletin is that all events with sufficient data are manually checked and relocated by experienced analysts. Therefore, the latest earthquake information in the database is 2 years behind in real-time. It also presents the event parameters reported by the contributor agencies and centers. The ISC finished rebuilding the entire database in 2020 by utilizing a new location algorithm (Bondár and Storchak, 2011) with the ak135 seismic velocity model (Kennett et al., 1995). Furthermore, previously unavailable hypocenter and station phase readings from the temporary and permanent networks are used to the rebuild bulletin (Storchak et al., 2017; International Seismological Centre, 2021). Therefore, the latest, most recent, and revised international dataset is used in this study. The earthquake parameters in the bulletin are in the IASPEI Seismic Format (available at: http://www.isc.ac.uk/standards/isf/). The overall data processing is given in the flowchart in **Figure 5**. Because the bulletin may contain multiple hypocenters from multiple agencies for an event, the ISC considers that one of them is primary and assigns to it the PRIME flag. A hypocenter determined by the ISC always has the PRIME flag. The parameters reported by the ISC are preferred first. If there is no information from the ISC, the availability of the hypocenter parameters from the European-Mediterranean Seismological Centre (EMSC or CSEM) is searched (see **Appendix A** for the institute abbreviations). The priority of both institutes is high because they use all available data in the study area.

## 7 METHODS AND DATA ANALYSIS

The ZMAP software package (Wiemer, 2001) available at http://www.earthquake.ethz.ch/ software/zmap has been utilized to perform the statistical analyses on the compiled data set. It includes a set of tools operated by a graphical user interface (GUI) and intended to help scientist in their analyses of catalog data. ZMAP is primarily a tool used to evaluate the quality of catalogs and to address assumptions. It was first published in

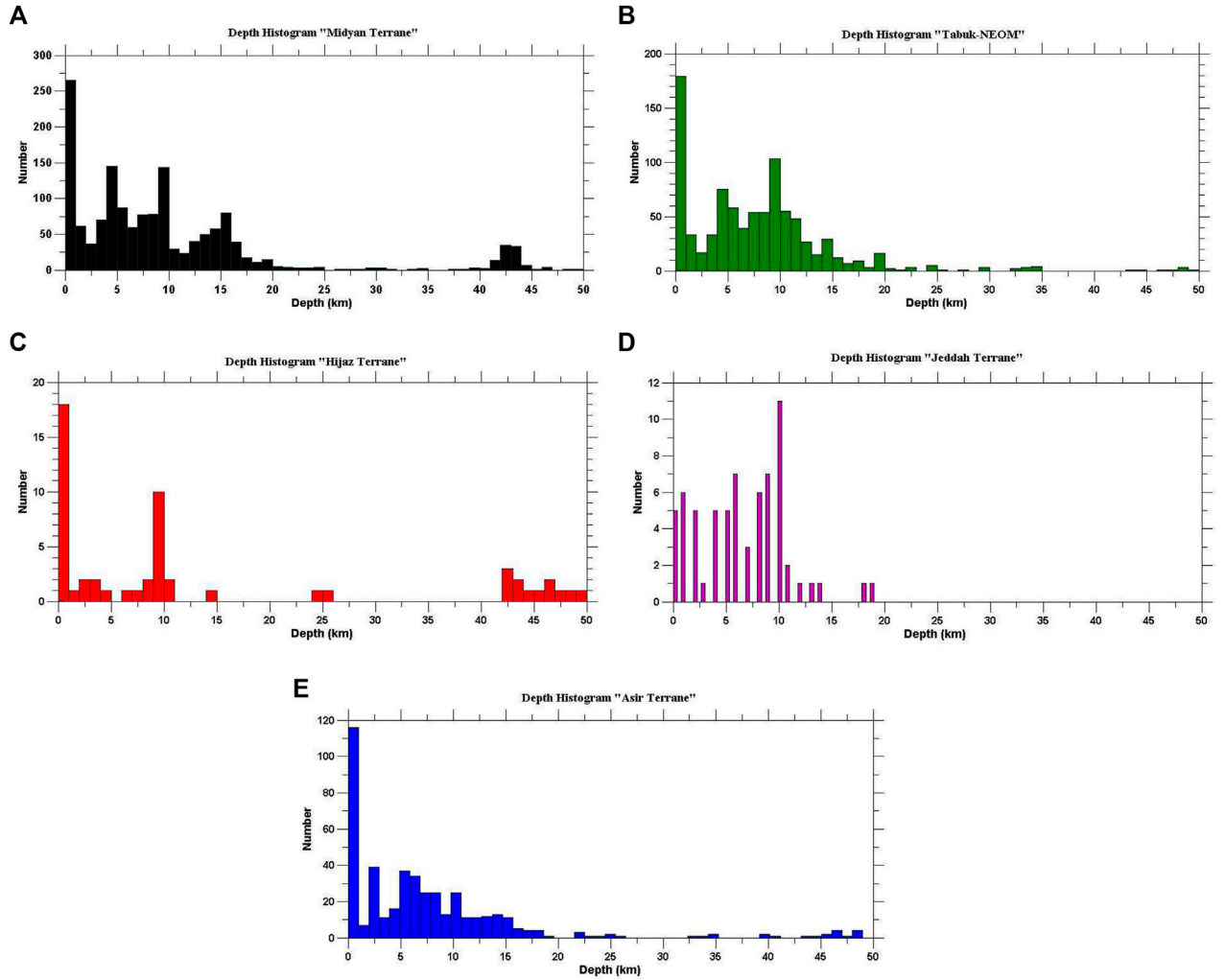


**FIGURE 10 | (A–E)** Depth histograms for the studied regions as represented by the color legend.

1994 then became well known over the last few years. It includes important features for the catalog quality assessment, such as artifacts, completeness, and contamination of explosion as well as interactive data exploration, stress tensor inversions, mapping transients in seismicity (b-values and rate changes) and fractal dimension analysis. The code of ZMAP is an open source, written in Matlab by the Mathworks, which is a widely used software language in the natural sciences. The ongoing renovation process of Zmap tools, which started as simple graphical retrofits, has evolved to leverage modern MATLAB's new graphics system, improved object-oriented capabilities, updated toolboxes, and has resulted in a version of ZMAP that provides vastly improved usability, speed, and reliability. Nearly every aspect of the ZMAP has been modified and is now compatible with MATLAB R2018a and later. The user interfaces have been modified to provide consistency and a high degree of interactivity.

The statistical analyses have been performed on the whole dataset of the Arabian Shield as a one region before subdividing it into terranes (**Figure 6**). The evolutions among the levels of seismic activities, i.e., the cumulative number of earthquakes plotted against time, are shown in **Figure 6A**. This evolution indicates the sudden increase in the cumulative seismicity curves of the Arabian Shield in 2004 and 2018. The a- and b- values, which may exhibit some differences based on the tectonic characteristics of the investigation area, were calculated for the Arbian Shield using the magnitude–frequency relationship (**Figure 6B**). The obtained a- and b-values were 4.53 and 0.64, respectively. The estimated magnitude of completeness for the whole catalog of the Arabian shield was Mc = 2.4. The magnitude histogram (**Figure 6C**) shows that the average magnitudes are between 1 and 3.4. The depth distribution (**Figure 6D**) shows that the depths of the vast majority of events in the catalog are between 0 and 15 km. The seismic activities between 40 and50 km have also been reported. The predominant depths are about 0–10 km. The time histogram (**Figure 6E**) displays the increase of seismic activity in 2004 and 2018–2019. There are very low activities that have been noticed in the period between 2013 and 2017.

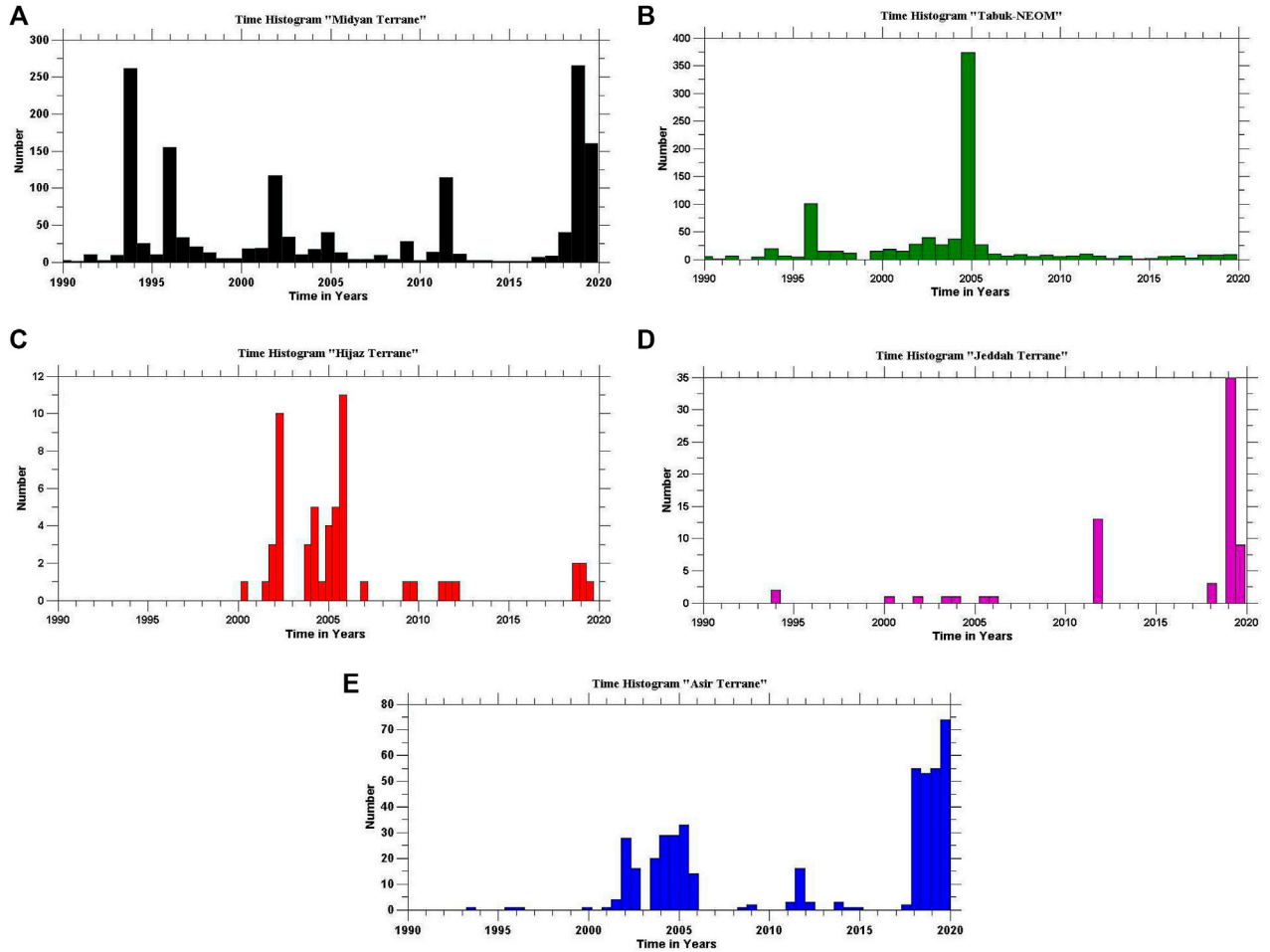


**FIGURE 11 | (A–E)** Time histograms for the studied regions as represented by the color legend.

In order to ensure a time-independent Poissonian distribution of seismicity, the earthquakes that occurred in clusters, such as foreshocks/aftershocks sequences and swarms, are aimed to be identified and then removed from the catalog. This process called the declustering process, in which earthquake clusters are usually defined by their proximity in time and space. Several approaches can be used for the declustering process (e.g., stochastic, deterministic = linking, and windowing methods). The windowing methods, such as the Gardner and Knopoff (1974) and Reasenberg (1985) are capable of identifying in a straightforward way the foreshock/mainshock/aftershock sequences, simply by applying the windows forward and backward in time from the mainshock. These methods do not distinguish between different generation of aftershocks (i.e., first generation resulting from the mainshock and those associated to previous aftershocks), and it is assumed that all dependent events would occur within the window. Also, they assumed a circular spatial window searching not full consistent with fault extension for larger magnitude earthquakes. We then used the most widely applied deterministic approach (Gardner and Knopoff, 1974), which is based on a windowing algorithm originally conceived for Southern California, but later adopted/modified to be used across the world (Uhrhammer, 1986; Stiphout et al., 2012). This method takes into consideration the tectonic context and related seismicity present in the region (active shallow, stable, and interface/inslab subduction) in order to decluster the catalog.

The distribution of events through time and latitude showing the foreshock, mainshock, aftershock sequences after applying the declustering for the subduction region are presented in **Figure 7**, together with window sizes (distance and time) with respect to the magnitude used by declustering methods. The declustering found a total of 759 (20.24%) clustered events out of 3,750. The map window now displays the declustered catalog containing 2,991 events as blue dots. The individual clusters are displayed as magenta pluses (**Figure 7**). The magnitude histogram of the declustered catalog is shown in **Figure 7C**. It shows a noteworthy difference from the magnitude histogram distributed by the data of the whole catalog (**Figure 6C**), which highlights the importance of the declustering process.

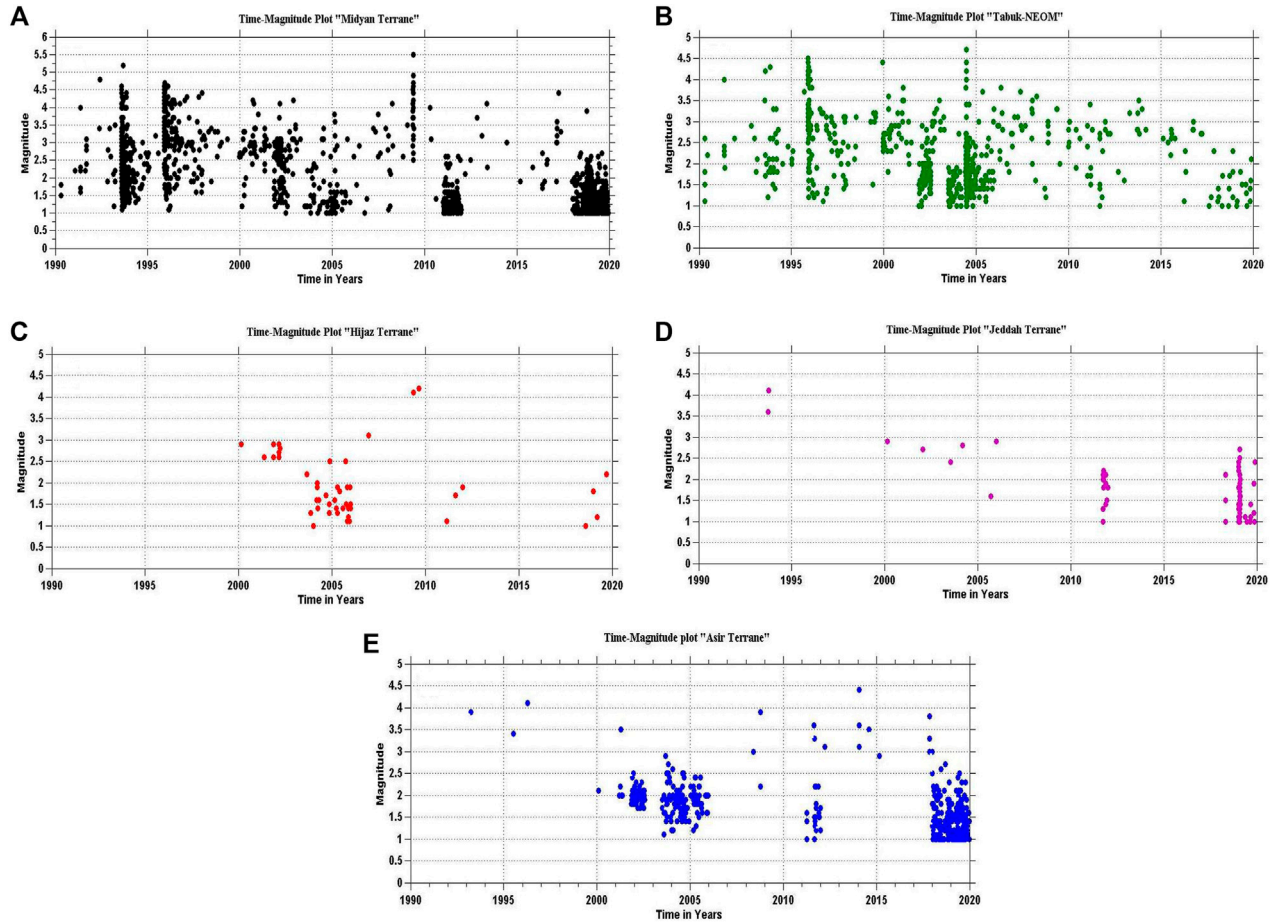


**FIGURE 12 | (A–E)** Time–magnitude distributions for the studied regions as represented by the color legend.

## 8 RESULTS

The Arabian Shield has been subdivided into five regions (The Midyan terrane, the Tabuk-Neom area, the Hijaz terrane, the Jeddah terrane, and the Asir terrane). The purpose of this study is to characterize the seismic activities related to these main terrains in the Arabian Shield. Furthermore, to indicate the dominant tectonic regimes of the studied regions and identify their related faulting types as well as characterize the earthquake rate changes and the risk of higher magnitude earthquakes related to each terrane and obtain some seismicity parameters [a- and b-values and magnitude of completeness (Mc)] and seismic hazard parameters (earthquake recurrence and maximum expected magnitude) to be able to perform actions for seismic risk reduction in the studied region.

For this purpose, we estimated the parameters from the deviation of the earthquake frequency–magnitude distribution from the Gutenberg–Richter law in each region (**Figure 8**). The a- and b-values, which may exhibit some differences based on the tectonic characteristics of the investigation areas, were calculated for each source region along with the magnitude–frequency relationship (**Figure 8** and **Table 1**). Among all the investigated areas, the highest b-values are detected in the Hijaz terrane (b = 1.04), while the lowest b-values were recorded in the Midyan terrane (b = 0.53). A reliable estimate of Mc is to define the point of the maximum curvature as the Mc by computing the maximum value of the first derivative of the frequency–magnitude curve. In practice, this matches the magnitude bin with the highest frequency of events in the noncumulative frequency–magnitude distribution (triangle symbols in **Figure 8**). Using the maximum curvature, which simply computes the maximum value of the first derivative of the FMD curve, the higher Mc values of 2.3 and 2.4 are obtained at the Hijaz terrane and Tabuk-Neom, respectively, while the lower values of Mc are of 1.4 for Midyan and Jeddah terranes. The obtained Mc values for all studied regions are given in **Table 1**.

The magnitude histograms illustrated in **Figure 9** shows that Midyan, Tabuk, and Asir Terranes have the higher seismicity at the study area with average magnitudes of 1.0–4.1 at Midyan, 1.0–3.3 at Tabuk, and 1.0–2.2 at Asir Terranes. The depth distributions (**Figure 10**) show that most earthquakes in the catalog occurred in shallow depths. The predominant depth ranges between 0 and 15 km. Hijaz and Jeddah Terranes show lower depth distributions. The yearly seismic rate histograms

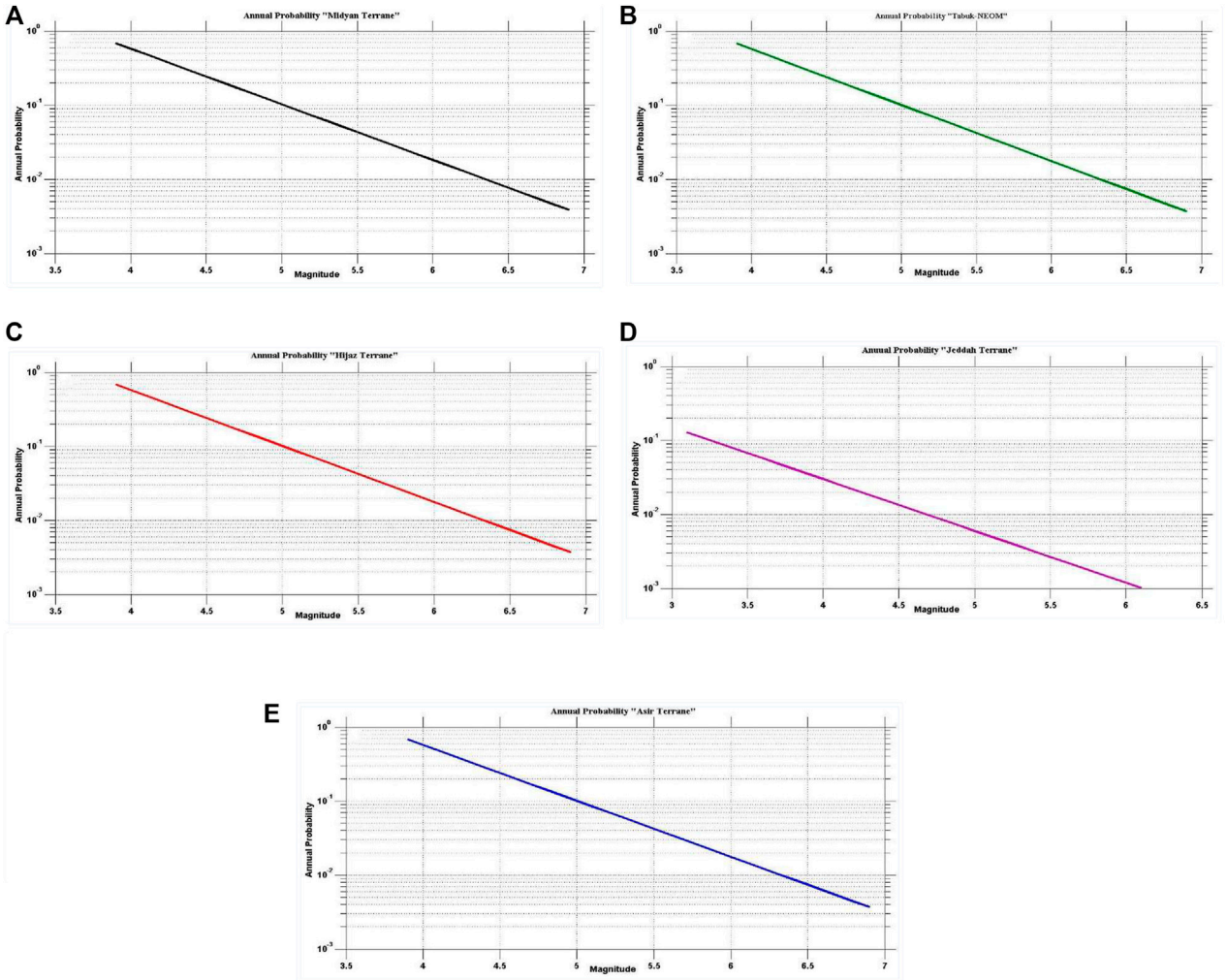


**FIGURE 13 | (A–E)** Annual probabilities of the earthquake activities in various levels of magnitude for the studied regions as represented by the color legend.

(**Figure 11**) display the higher seismic activity periods in 1993, 1995, 2001–2002, 2011, and 2017–2019 (Midyan), in 2005 (Tabuk), between 2002 and 2006 (Hijaz), in 2011 and between 2019 and 2020 (Jeddah), and between 2001 and2006 and 2017 and 2020 (Asir). The Magnitude rate distribution of the earthquakes (**Figure 12**) reveals an important increase in the number of large magnitude earthquakes in the period between 1993 and2009 in Midyan terrain, in 1996 and 2004 in Tabuk. Two events above magnitude 4.0 unlike the normal moderate activity with magnitudes below 3.0 are recorded in Hijaz terrane. The same for the Jeddah terrane, where most of the seismicity are below 3.0, except in 1994, where two events with magnitudes above 3.5 are reported. A random slight increase in magnitude is observed at Asir terrane from time to time.

The probability of occurrence of earthquakes of various magnitudes in certain time intervals is of the highest rate in Midyan terrane and lowest in Jeddah terrane (**Figure 13**), while the returned periods were found to be higher in Jeddah terrane and lowest in Midyan terrane (**Figure 14**). The maximum expected magnitudes (Mmax) are found to be 6.0 for Midyan terrane, 5.4 for Tabuk-Neom, 4.7 for Hijaz terrane, 4.8 for Jeddah terrane, and 7.7 for Asir terrane. The average recurrence intervals of earthquakes with the Mmax are ~7, ~20, ~6, ~120, and ~200 years for each seismic terrane, respectively.

## 9 DISCUSSION AND CONCLUSION

In the context of tectonic plate movements, complex structural patterns within the Arabian Plate related to the collision between Arabian and Eurasian plates have been interpreted. The slowing of the convergence or the onset of collision between Arabia and Eurasia, as well as the change in Africa–Eurasia motion may be reflected by a stepping of the locus of extension from the spreading axis to off axis dikes and temporarily correlated with the onset of volcanism within the western Arabian margin (Aldaajani et al., 2021).

Several geophysical studies indicate that the Arabian Shield is an active seismic region (Al-Noury and Ali, 1986; Al-Haddad

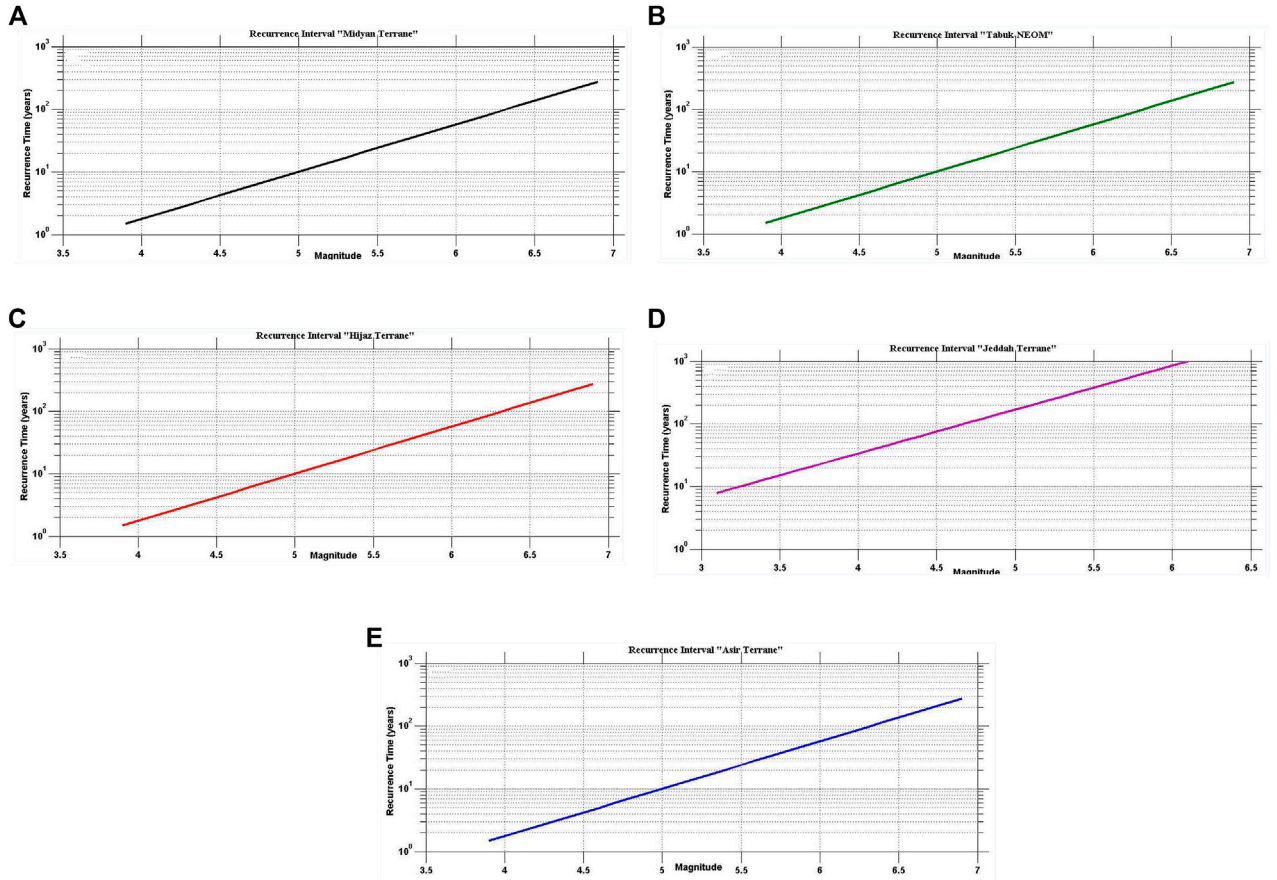


**FIGURE 14 | (A–E)** The recurrence interval for all earthquake magnitudes as represented by the color legend.

et al., 1994; Al-Amri, 2013; Youssef, 2015). The rapid economic expansion in the region has resulted in industrial development and intensive urbanization, with large engineering structures and projects already constructed, under construction, or being planned, such as dams for irrigation and power, desalination plants, and nuclear power plants.

The most recently compiled focal mechanism solutions of 122 earthquakes with $3.7 \leq ml \leq 7.1$ and depth ranges between 0 and 30 km demonstrate a dominant normal faulting mechanism with a minor component of strike-slip motion and the two nodal planes trending NW-SE. This type of mechanism presents the tectonic movement of the region and the NW-SE trend is consistent with the common trending faults. The dominantly extensional tectonic regime with nearly horizontal NE-SW trending delineates the influence of NE extension in the Red Sea. This stress system reactivated the preexisting lineaments of the Najd fault system, which was active during the Precambrian, and was reactivated several times during the geological history of the region (Agar, 1987; Stern, 1994). The above results get on well with the geological observations (Roobol, 2007) that exhibit that the Red Sea passive margin is undergoing extension by rotational normal faulting dipping both toward and away from the Red Sea that cause thinning of the Arabian Shield.

In order to determine the earthquake occurrences and earthquake recurrence characteristics in the study area, an initial earthquake dataset containing 3,750 seismic events recorded between 1941 and 2019 with magnitudes of 1.0 and 6.2 and depths between 0 and 50 km was examined. The statistical analyses have been performed on the whole dataset and the results demonstrate the sudden increase in the cumulative seismicity curves of the Arabian Shield in 2004 and 2018. The obtained a- and b-values were 4.53 and 0.64, respectively. The estimated magnitude of completeness was Mc = 2.4. The average magnitudes were estimated between 1 and 3.4. The predominant depths are about 0–10 km, and seismic activities in depths between 40 and 50 km with exceedingly low strain rates were also noticed. These activities could be within the lithospheric mantle where Volcanic fields in the mantle and lower-crustal zones are located. An increase of seismic activity in 2004 and 2018–2019 was displayed, and very low activities were noticed in the period between2013 and 2017.

In the current study all inadequate data of the catalog, as well as the aftershocks have been taken off, and each earthquake cluster has been replaced by an equivalent event using the declustering technique represented by Gardner and Knopoff (1974). Finally, a declustered earthquake catalog includes 2,991 earthquakes has been used to characterize the seismicity of the

study area. Keeping in view the prevalent tectonics and the geological, geophysical, and seismological data, the study area is represented by five zones (terranes) include Midyan terrane, Tabuk-Neom, Hijaz terrane, Jeddah terrane and Asir terrane.

The distributions of spatial magnitudes along the study area denote higher seismic activity records at the northwestern part of Arabian Shield, especially at Midyan and Tabuk-Neom with average magnitudes of 1.0–4.1 and 1.0–3.3, respectively, as well as at the southeastern Saudi Arabia at Asir terrane with an average magnitude of 1.0–2.2. Low seismic activities have been observed at Hijaz and Jeddah terranes. The temporal migrations of seismicity along the depth axis indicate that the seismic activity of the study area is concentrated in the upper crust zone in a shallow depth between 0 and 15 km.

In the current study, the maximum likelihood technique was applied to specify the seismicity of the areas under study and to calculate their associated seismicity parameters [Gutenberg–Richter (GR) recurrence parameters (a- and b-values) and the Magnitudes of completeness (Mc)]. Compared with the least-square regression method, this method gives more reasonable results (Aki, 1965). The ZMAP software has been used to compute Mc, a- and b-values. The results showed that the a-values varied between 2.70 and 4.35, and the b-values varied between 0.50 and 1.04.

The variations of the defined a- and b- values through the study regions not only reflect the geodynamic processes such as seafloor spreading and continental rift but also assess the seismic hazard that threatens the megaprojects in the regions such as the Red Sea Development and Neom. The highest b-value was determined in the Hijaz terrane (b = 1.04), which suggests that it is associated with a decreased risk of higher magnitude earthquakes. The lowest b-value was estimated in the Midyan terrane (b = 0.53) that indicates the higher risk of larger magnitude earthquakes. Since b-value is inversely related to stress (Woessner and Wiemer, 2005), so the Hijaz terrane is associated with low stress regime. This indicates the faults of this source zone are capable to generate numerous smaller magnitude earthquakes of short return periods, which agrees with the estimated maximum magnitude of ml = 4.7. In contrast, the Midyan terrane indicates high stress regime that may have high hazard of large magnitude earthquakes of large return periods, which is confirmed by the estimated maximum magnitude of ml = 6.0. The higher Mc values of 2.3 and 2.4 are obtained at the Hijaz terrane and Tabuk-Neom, respectively, while the lower values of Mc are of 1.4 for Midyan and Jeddah terranes. The lower value of Mc at the Midyan terrane demonstrates appropriate station distribution and high earthquake rates. However, at the Jeddah terrane the seismic activities are poorly detected (with only 68 events over magnitude 1.0) that probably leads to the small value of Mc. Mc thresholds in the Hijaz terrane and Tabuk-Neom are with higher values, where the station distribution is very poor.

The probability of occurrence and return periods for earthquakes of various magnitudes in each terrane indicate that the regions related to the Najd strike-slip fault system are probably the regions for large earthquake occurrences.

The results of the current study demonstrate the influence of tectonic activities, geodynamic processes, thickness of the crust, the active volcanic field in the lithospheric mantle, and the multiple directions of the faults and their densities and stresses on the locations and depths of the seismic activities in each terrane of the Arabian Shield. These results are consistent with the previous studies that have been done in the study area and surrounding regions, such as Al-Amri et al., 2004; El-Hadidy et al., 2015; Zahran et al., 2016; Alzahrani et al., 2022.

## DATA AVAILABILITY STATEMENT

The original contributions presented in the study are included in the article/Supplementary Material. Further inquiries can be directed to the corresponding author.

## AUTHOR CONTRIBUTIONS

SA gathered, retrieved, processed, analyzed, and interpreted the data, created and edited the figures, and was a contributor in writing and editing the manuscript. KA brought the idea of the research, gathered the structure, tectonic, and seismicity of the study area, plotted the study region map, and was a contributor in writing and editing the manuscript. All authors read and approved the final version of the manuscript.

## FUNDING

This study was financed by the Researchers Supporting Project number (RSP-2021/351), King Saud University, Riyadh, Saudi Arabia. Funds are received for open access publication fees.

## ACKNOWLEDGMENTS

Sincere thanks and gratitude to the Researchers Supporting Project number (RSP-2021/351), King Saud University, Riyadh, Saudi Arabia, for funding this research article. The authors are grateful to the reviewers and the handling editor for their constructive comments and suggestions.

## REFERENCES

Agar, R. A. (1987). The Najd Fault System Revisited; a Two-Way Strike-Slip Orogen in the Saudi Arabian Shield. *J. Struct. Geology.* 9, 41–48. doi:10.1016/0191-8141(87)90042-3

Aki, K. (1965). Maximum Likelihood Estimates of B in the Formula Log N=a-bM and its Confidence Limits. *Bull. Earthq. Res. Inst. Univ. Tokyo* 43, 237–239.

Al-Amri, A. M., Punsslan, B. T., Khalil, A., and Uy, E. A. (2004). *Seismic hazard Assessment of Western Saudi Arabia and the Red Sea Region*. Japan: IISEE, 95–112.

Al-Amri, A. M. (2013). "Seismotectonics and Seismogenic Source Zones of the Arabian Platform," in *Lithosphere Dynamics and Sedimentary Basins: The Arabian Plate and Analogues*. Editors K. Al Hosani, F. Roure, R. Ellison, and S. Lokier (Springer Frontiers in Earth Sciences), 295–316. doi:10.1007/978-3-642-30609-9-1510.1007/978-3-642-30609-9_15

Al-Haddad, M., Siddiqi, G. H., Al-Zaid, R., Arafah, A., Necioglu, A., and Turkelli, N. (1994). A Basis for Evaluation of Seismic hazard and Design Criteria for Saudi Arabia. *Earthquake Spectra* 10, 231–258. doi:10.1193/1.1585773

Al-Malki, M. A., and Al-Amri, A. M. (2013). "Seismic Zones Regionalization and hazard Assessment of SW Arabian Shield and Southern Red Sea Region," in *Lithosphere Dynamics and Sedimentary Basins: The Arabian Plate and Analogues* (Springer), 317–331. doi:10.1007/978-3-642-30609-9_16

Al-Noury, S., and Ali, S. (1986). Seismic Risk Analysis of Western Arabia. *Eng. Geology.* 23, 95–108. doi:10.1016/0013-7952(86)90032-3

Aldaajani, T. Z., Almalki, K. A., and Betts, P. G. (2021). Plume versus Slab-Pull: Example from the Arabian Plate. *Front. Earth Sci.* 9, 494. doi:10.3389/feart.2021.700550

Ali, S. M., and Akkoyunlu, M. F. (2022). Statistical Analysis of Earthquake Catalogs for Seismic hazard Studies Around the Karliova Triple Junction (Eastern Turkey). *J. Afr. Earth Sci.* 186, 104436. doi:10.1016/j.jafrearsci.2021.104436

Ali, S. M., and Shanker, D. (2017). Study of Seismicity in the NW Himalaya and Adjoining Regions Using IMS Network. *J. Seismol.* 21, 317–334. doi:10.1007/s10950-016-9603-7

Ali, S. M. (2016). Statistical Analysis of Seismicity in Egypt and its Surroundings. *Arab J. Geosci.* 9, 52. doi:10.1007/s12517-015-2079-x

Alzahrani, H., Abdelrahman, K., Qaysi, S., and Baras, M. (2022). Seismicity of the Neom Megaproject Area, Northwestern Saudi Arabia. *J. King Saud Univ. - Sci.* 34, 101659. doi:10.1016/j.jksus.2021.101659

Ambraseys, N. N., and Adams, R. D. (1988). *The Seismicity of Saudi Arabia and Adjacent Areas: Part B. ICST/ KACST Project*. ESEE Rep. no. 88/11. London: Dept. of Civil Engineering, Imperial College of Science and Technology.

Ambraseys, N. N., Melville, C. P., and Adams, R. D. (1994). *The Seismicity of Egypt, Arabia and the Red Sea: A Historical Review*. Cambridge: Cambridge University Press.

Ambraseys, N. N., and Melville, C. P. (1989). Evidence for Intraplate Earthquakes in Northwestern Arabia. *Bull. Seism Soc. Am.* 79, 1279–1281.

Ambraseys, N. N., and Melville, C. P. (1988). *The Seismicity of Saudi Arabia and Adjacent Areas: Part A. ICST/ KACST Project*. ESEE Rep. no. 88/11. London: Dept. of Civil Engineering, Imperial College of Science and Technology.

ArRajehi, A., McClusky, S., Reilinger, R., Daoud, M., Alchalbi, A., Ergintav, S., et al. (2010). Geodetic Constraints on Present-Day Motion of the Arabian Plate: Implications for Red Sea and Gulf of Aden Rifting. *Tectonics* 29 (3), TC3011 (1–10). doi:10.1029/2009tc002482

Beydoun, Z. R. (1999). Evolution and Development of the Levant (Dead Sea Rift) Transform System: A Historical-Chronological Review of a Structural Controversy. *Geol. Soc. Lond. Spec. Publ.* 164 (1), 239–255. doi:10.1144/gsl.sp.1999.164.01.12

Bondár, I., and Storchak, D. (2011). Improved Location Procedures at the International Seismological Centre. *Geophys. J. Int.* 186, 1220–1244. doi:10.1111/j.1365-246X.2011.05107.x

Brown, G. F. (1970). A Discussion on the Structure and Evolution of the Red Sea and the Nature of the Red Sea, Gulf of Aden and Ethiopia Rift junction - Eastern Margin of the Red Sea and the Coastal Structures in Saudi Arabia. *Phil. Trans. R. Soc. Lond. A.* 267, 75–87. doi:10.1098/rsta.1970.0024

Davidson, I., Al-Kadasi, M., Al-Kihrbash, A., Baker, J., Blakey, S., Bosence, D., et al. (1994). Structural Evolution of the southeastern Red Sea Margin, Republic of Yemen. *Geol. Soc. Am. Bull.* 106, 1474–1493.

Efron, B. (1979). Bootstrap Methods: Another Look at the Jackknife. *Ann. Statist.* 7, 1–26. doi:10.1214/aos/1176344552

El-Hadidy, S. Y., Zahran, H. M., El-Hadidy, M., and Sami, M. (2015). "Seismicity and Seismotectonic Settings of Western Saudi Arabia with Special Emphasis of 5.1 Baish-Jizan Earthquake 2014," in Workshop on Imaging and Active Tectonics of the Red Sea Region, Kingdom of Saudi Arabia, March 10-13, 2015 (King Abdulaziz University of Science and Technology KAUST).

El-Isa, Z. H., and Shanti, A. A. (1989). Seismicity and Tectonics of the Red Sea and Western Arabia. *Geophys. J.* 97, 449–457. doi:10.1111/j.1365-246x.1989.tb00515.x

Frankel, A. (1995). Mapping Seismic hazard in the Central and Eastern United States. *Seismol. Res. Lett.* 66 (4), 8–21. doi:10.1785/gssrl.66.4.8

Frohlich, C., Gan, W., and Herrmann, R. B. (2015). Two Deep Earthquakes in Wyoming. *Seismol. Res. Lett.* 86, 810–818. doi:10.1785/0220140197

Gardner, J. K., and Knopoff, L. (1974). Is the Sequence of Earthquakes in Southern California, with Aftershocks Removed, Poissonian? *Bull. Seismol. Soc. Am.* 64 (5), 1363–1367. doi:10.1785/bssa0640051363

Genna, A., Nehlig, P., Le Goff, E., Guerrot, C., and Shanti, M. (2002). Proterozoic Tectonism of the Arabian Shield. *Precambr. Res.* 117, 21–40. doi:10.1016/s0301-9268(02)00061-x

Ghebreab, W. (1998). Tectonics of the Red Sea Region Reassessed. *Earth Sci. Rev.* 45, 1–44. doi:10.1016/S0012-8252(98)00036-1

Girdler, R. W. (1991). The Afro-Arabian Rift System-An Overview. *Tectonophysics* 197, 139–153. doi:10.1016/0040-1951(91)90038-t

Gutenberg, R., and Richter, C. F. (1944). Earthquake Magnitude, Intensity, Energy, and Acceleration. *Bull. Seismol Soc. Am.* 32, 163–191.

Hafiez, H. E. A., and Toni, M. (2020). Magnitude of Completeness for the Northern Stations of the Egyptian National Seismological Network. *Arab J. Geosci.* 13 (12), 458–461. doi:10.1007/s12517-020-05461-0

International Seismological Centre (ISC) (2021). On-line Bulletin. Available at: http://www.isc.ac.uk/iscbulletin/search/catalogue/. doi:10.31905/D808B830

Jamali, F., Aghda, S. M. F., and Aliyari, A. (2006). *Evaluation of Seismic Sources for hazard Assessment in the Fujairah Emirate (UAE)*. London, UK: The Geological Society of London. IAEG2006, 305 (1–6).

Johnson, P. R. (1998). *Tectonic Map of Saudi Arabia and Adjacent areasMinistry of Petroleum and Mineral Resources*. Jiddah, Saudi Arabia: Deputy Ministry for Mineral Resources. Technical Report USGS TR-98-3 (IR 948).

Kennett, B. L. N., Engdahl, E. R., and Buland, R. (1995). Constraints on Seismic Velocities in the Earth from Traveltimes. *Geophys. J. Int.* 122, 108–124. doi:10.1111/j.1365-246x.1995.tb03540.x

Kijko, A. (2004). Estimation of the Maximum Earthquake Magnitude, M max. *Pure Appl. Geophys.* 161, 1655–1681. doi:10.1007/s00024-004-2531-4

Klinger, Y., Rivera, L., Haessler, H., and Maurin, J.-C. (1999). Active Faulting in the Gulf of Aqaba: New Knowledge from the Mw 7.3 Earthquake of 22 November 1995. *Bull. Seismol Soc. Am.* 89, 1025–1036. doi:10.1785/bssa0890041025

Kröner, A. (1985). Ophiolites and the Evolution of Tectonic Boundaries in the Late Proterozoic Arabian-Nubian Shield of Northeast Africa and Arabia. *Precambr. Res.* 27, 277–300. doi:10.1016/0301-9268(85)90016-6

Leonard, T., Papasouliotis, O., and Main, I. G. (2001). A Poisson Model for Identifying Characteristic Size Effects in Frequency Data: Application to Frequency-Size Distributions for Global Earthquakes, "starquakes", and Fault Lengths. *J. Geophys. Res.* 106 (B7), 13473–13484. doi:10.1029/2000jb900429

Manakou, M. V., and Tsapanos, T. M. (2000). Seismicity and Seismic hazard Parameters Evaluation in the Island of Crete and the Surrounding Area Inferred from Mixed Data Files. *Tectonophysics* 321, 157–178. doi:10.1016/s0040-1951(00)00075-5

Michael, A. J. (2014). How Complete Is the ISC-GEM Global Earthquake Catalog? *Bull. Seismol. Soc. Am.* 104, 1829–1837. doi:10.1785/0120130227

Mignan, A., Werner, M. J., Wiemer, S., Chen, C. C., and Wu, Y. M. (2011). Bayesian Estimation of the Spatially Varying Completeness Magnitude of Earthquake Catalogs. *Bull. Seismol. Soc. Am.* 101, 1371–1385. doi:10.1785/0120100223

Mignan, A., and Woessner, J. (2012). *Estimating the Magnitude of Completeness for Earthquake Catalogs*. Community Online Resource for Statistical Seismicity Analysis. ETH Zurich: Swiss Seismological Service, 45. Available at: http://www.corssa.org. doi:10.5078/corssa-00180805

Mogi, K. (1962). Magnitude–frequency Relationship for Elastic Shocks Accompanying Fractures of Various Materials and Some Related Problems in Earthquakes. *Bull. Earthq Res. Inst. Univ. Tokyo* 40, 831–883.

Petersen, M. D., Bryant, W. A., Cramer, C. H., Cao, T., Reichle, N. S., Frankel, A. D., et al. (1996). *Probabilistic Seismic hazard Assessment for the State of California*. Open-File Report 96–08, USGS Open File Report 96–706. California, USA: California Dept. of Conservation Division of Mines and Geology. doi:10.3133/ofr96706

Prieto, G. A., Froment, B., Yu, C., Poli, P., and Abercrombie, R. (2017). Earthquake Rupture below the Brittle-Ductile Transition in continental Lithospheric Mantle. *Sci. Adv.* 3, e1602642. doi:10.1126/sciadv.1602642

Reasenberg, P. (1985). Second-order Moment of central California Seismicity, 1969-1982. *J. Geophys. Res.* 90, 5479–5495. doi:10.1029/jb090ib07p05479

Reilinger, R., McClusky, S., Vernant, P., Lawrence, S., Ergintav, S., Cakmak, R., et al. (2006). GPS Constraints on continental Deformation in the Africa-Arabia-Eurasia continental Collision Zone and Implications for the Dynamics of Plate Interactions. *J. Geophys. Res.* 111, B05411 (1–26). doi:10.1029/2005jb004051

Roobol, J. (2007). "Cenozoic Faults in Western Saudi Arabia," in 7th meeting of the Saudi society for geosciences, Riyadh, Saudi Arabia (King Saud University).

Rydelek, P. A., and Sacks, I. S. (1989). Testing the Completeness of Earthquake Catalogues and the Hypothesis of Self-Similarity. *Nature* 337, 251–253. doi:10.1038/337251a0

Scholz, C. H. (1968). The Frequency-Magnitude Relation of Microfracturing in Rock and its Relation to Earthquakes. *Bull. Seismol Soc. Am.* 58, 399–415. doi:10.1785/bssa0580010399

Schorlemmer, D., Wiemer, S., and Wyss, M. (2005). Variations in Earthquake-Size Distribution across Different Stress Regimes. *Nature* 437 (7058), 539–542. doi:10.1038/nature04094

Sharland, P. R., Archer, R., Casey, D. M., Davies, R. B., Hall, S. H., Heward, A. P., et al. (2001). *Arabian Plate Sequence Stratigraphy*, 2. Bahrain: GeoArabia Special Publication, 371.

Stern, R. J. (1994). Arc Assembly and continental Collision in the Neoproterozoic East African Orogen: Implications for the Consolidation of Gondwanaland. *Annu. Rev. Earth Planet. Sci.* 22, 319–351. doi:10.1146/annurev.ea.22.050194.001535

Stern, R. J., and Johnson, P. (2010). Continental Lithosphere of the Arabian Plate: a Geologic, Petrologic, and Geophysical Synthesis. *Earth-Science Rev.* 101, 29–67. doi:10.1016/j.earscirev.2010.01.002

Stiphout, T. v., Zhuang, J., and Marsan, D. (2012). "Theme V -Models and Techniques for Analysing Seismicity,". Technical report in *Community Online Resource for Statistical Seismicity Analysis*. Available at: http://www.corssa.org.

Stoeser, D. B., and Camp, V. E. (1985). Pan-African Microplate Accretion of the Arabian Shield. *Geol. Soc. Am. Bull.* 96, 817–826. doi:10.1130/0016-7606(1985)96<817:pmaota>2.0.co;2

Storchak, D. A., Harris, J., Brown, L., Lieser, K., Shumba, B., Verney, R., et al. (2017). Rebuild of the Bulletin of the International Seismological Centre (ISC), Part 1: 1964-1979. *Geosci. Lett.* 4 (32), 1–14. doi:10.1186/s40562-017-0098-z

Uhrhammer, R. (1986). Characteristics of Northern and Central California Seismicity. *Earthquake Notes* 57.1, 21.

Walpersdorf, A., Hatzfeld, D., Nankali, H., Tavakoli, F., Nilforoushan, F., Tatar, M., et al. (2006). Difference in the GPS Deformation Pattern of North and Central Zagros (Iran). *Geophys. J. Int.* 167 (3), 1077–1088. doi:10.1111/j.1365-246x.2006.03147.x

Wells, D. L., and Coppersmith, K. J. (1994). New Empirical Relationships Among Magnitude, Rupture Length, Rupture Width, Rupture Area, and Surface Displacement. *Bull. Seismol Soc. Am.* 84, 974–1002.

Wiemer, S. (2001). A Software Package to Analyze Seismicity: ZMAP. *Seismol. Res. Lett.* 72, 373–382. doi:10.1785/gssrl.72.3.373

Wiemer, S., and Wyss, M. (2000). Minimum Magnitude of Completeness in Earthquake Catalogs: Examples from Alaska, the Western United States, and Japan. *Bull. Seismol. Soc. Am.* 90, 859–869. doi:10.1785/0119990114

Woessner, J., and Wiemer, S. (2005). Assessing the Quality of Earthquake Catalogues: Estimating the Magnitude of Completeness and its Uncertainty. *Bull. Seismol. Soc. Am.* 95, 684–698. doi:10.1785/0120040007

Youssef, S. E.-H. (2015). "Seismicity and Seismotectonic Setting of the Red Sea and Adjacent Areas," in *The Red Sea*. Editors N. M. A. Rasul and I. C. F. Stewart (Berlin Heidelberg: Springer Earth System Sciences), 151–159. doi:10.1007/978-3-662-45201-1_8

Zahran, H. M., Sokolov, V., Roobol, M. J., Stewart, I. C. F., El-Hadidy Youssef, S., and El-Hadidy, M. (2016). On the Development of a Seismic Source Zonation Model for Seismic hazard Assessment in Western Saudi Arabia. *J. Seismol.* 20, 747–769. doi:10.1007/s10950-016-9555-y

**Author Disclaimer:** The views expressed on this paper are those of the authors and do not necessarily reflect the views of the organizations that the authors represent.

**Conflict of Interest:** The authors declare that the research was conducted in the absence of any commercial or financial relationships that could be construed as a potential conflict of interest.

**Publisher's Note:** All claims expressed in this article are solely those of the authors and do not necessarily represent those of their affiliated organizations, or those of the publisher, the editors, and the reviewers. Any product that may be evaluated in this article, or claim that may be made by its manufacturer, is not guaranteed nor endorsed by the publisher.

## APPENDIX A

The ISC contributor institutes mentioned in this study are given below. The ISS and GUTE catalogs are used for the events in the period of 1900–1964.

**Code** Institute

**ISC** International Seismological Centre

**ISS** International Seismological Summary [for 1900–1964]

**GUTE** Gutenberg and Richter (1954) [for 1900–1952]

**CSEM** European-Mediterranean Seismological Centre - EMSC (France)

**ISK** B.U. Kandilli Observatory and Earthquake Research Institute (Turkey)

**DDA** General Directorate of Disaster Affair (Turkey), until September 2017

**AFAD** Disaster and Emergency Management Presidency (Turkey), since October 2017

**ATH** National Observatory of Athens (Greece)

**THE** Dept. of Geophysics, Aristotle University of Thessaloniki (Greece)

**MOS** Geophysical Survey of Russian Academy of Sciences (Russia)

**TEH** Tehran University (Iran)

**TAB** Tabriz Seismological Observatory (Iran)

**TIF** Institute of Earth Sciences/ National Seismic Monitoring Center (Georgia)

**SOF** National Institute of Geophysics, Geology, and Geography (Bulgaria)

**BUC** National Institute for Earth Physics (Romania)

**SIGU** Subbotin Institute of Geophysics, National Academy of Sciences (Ukraine)

**IPER** Institute of Physics of the Earth, Academy of Sciences, Moscow (Russia)

**NSSP** National Survey of Seismic Protection (Armenia)

**AZER** Republican Seismic Survey Centre of Azerbaijan National Academy of Sciences (Azerbaijan)

**NSSC** National Syrian Seismological Centre (Syria)

**THR** International Institute of Earthquake Engineering and Seismology (Iran)